# $4f^n \rightarrow 4f^{n-1}5d$ transitions of the light lanthanides: Experiment and theory

L. van Pieterson,[1,*] M. F. Reid,[1,2] R. T. Wegh,[1] S. Soverna,[1] and A. Meijerink[1]
[1]*Debye Institute, Utrecht University, P.O. Box 80 000, 3508 TA Utrecht, The Netherlands*
[2]*Department of Physics and Astronomy, University of Canterbury, Christchurch, New Zealand*
(Received 13 November 2000; revised manuscript received 9 March 2001; published 10 January 2002)

The $4f^n \rightarrow 4f^{n-1}5d(fd)$ excitation spectra of the light lanthanides ($Ce^{3+}$, $Pr^{3+}$, $Nd^{3+}$, $Sm^{3+}$, and $Eu^{3+}$) incorporated in $LiYF_4$, $CaF_2$, and $YPO_4$ are investigated in the ultraviolet and vacuum-ultraviolet spectral region (100–250 nm). In these host lattices fine structure (zero-phonon lines and vibronic lines) is observed for *fd* transitions involving the lowest $5d$ crystal-field state. The observation of zero-phonon lines makes it possible to analyze the complicated structure in the *fd* spectra and to compare the experimentally observed spectra with energy-level calculations for the $4f^{n-1}5d$ states. Energy-level and intensity calculations were performed by an extension of the commonly used theory for energy-level calculations of $4f^n$ states. A good agreement between experiment and theory is obtained for the overall structure using the crystal-field splitting (from the spectra of $Ce^{3+}$), the parameters for the splitting of the $4f^{n-1}$ core (from the literature on energy level calculations for $4f^n$ states) and the spin-orbit coupling of the $5d$ electron and Coulomb interaction between $4f$ and $5d$ electrons (from atomic parameters using the computer code of Cowan).

DOI: 10.1103/PhysRevB.65.045113 PACS number(s): 78.40.Ha, 78.20.Bh, 71.55.−i, 71.70.Ch

## I. INTRODUCTION

The spectroscopy of the lanthanide ions is characterized by the observation of sharp, atomiclike lines (with linewidths of typically 1 $cm^{-1}$) in their absorption and emission spectra. These lines are due to intraconfigurational $4f^n$ transitions and have been studied extensively over the past several decades. This has resulted in a thorough understanding of many aspects of lanthanide luminescence and nowadays the energies and intensities for the transitions within the $4f^n$ configuration can be calculated using detailed theoretical models.[1–3] Much less is known about the interconfigurational $4f^n \rightarrow 4f^{n-1}5d(fd)$ transitions. The lack of research on *fd* transitions is partly caused by the fact that the transitions lie generally in the UV and vacuum-ultraviolet (VUV) regions, making them experimentally less accessible. In addition, since the lanthanide $5d$ orbitals are much more extended than the $4f$ orbitals, most of the intensity is in vibronic bands, making the spectra more difficult to analyze.

Recently there has been an increased effort in the study of the high-energy (vacuum-ultraviolet) spectroscopy of rare earth ions. Research on the vacuum-ultraviolet spectroscopy has been triggered by the need for new VUV phosphors and scintillator materials. For the $4f^n \rightarrow 4f^n$ transitions new energy levels were identified in the VUV and the well-known Dieke diagrams[4] have been extended from 40 000 to 65 000 $cm^{-1}$. The experimentally observed $4f^n$ levels could be well explained by energy level calculations,[5] confirming that the presently used theories for the calculations of energy levels within the $4f^n$ configuration are reliable. Also the *fd* excitation spectra have been measured for various lanthanides in the VUV and interesting new results have been obtained, such as the recent identification of spin-forbidden *fd* transitions for all heavy ($n>7$) rare earth ions in $LiYF_4$, which were previously only reported for $Tb^{3+}$ ($4f^8$).[6] Contrary to the situation for $4f^n$ states, energy level calculations for $4f^{n-1}5d$ states have, until recently, not been able to accurately reproduce the experimentally observed levels and the structure in the *fd* absorption spectra is still not well understood.

Some work has been done on *fd* spectra of the divalent lanthanides, especially $Sm^{2+}$, $Eu^{2+}$, and $Yb^{2+}$ (Ref. 7). For example, the absorption spectrum of $Eu^{2+}$ in $CaF_2$ shows two broad bands in the UV with a ''staircase'' structure.[8] Theoretical models have been proposed to account for this structure. Kaplyanskii *et al.* assigned the two broad structured bands to transitions from the $4f^7$ ground state of $Eu^{2+}$ to the $T_{2g}$ and $E_g$ excited states of the $4f^6 5d$ configuration.[9,10] They explained the structure of the bands by the splitting of the $4f^6$ core (assuming no interaction between the $4f^6$ core and the $5d$ electron). Support for this explanation comes from the observation that the distances between the peaks that compose the ''staircase'' structure agree with the energy spacing of the $Eu^{3+}$ multiplet. However, later it was shown that the Coulomb interaction of the *f* and *d* electrons cannot be assumed to be small[11–14] and models using both LS and *Jj* coupling were developed to explain the structure in the *fd* excitation spectra of divalent rare earths.

For the trivalent lanthanides systematic research on the *fd* excitation spectra is scarce, because the spectra extend into the VUV. An excellent overview of the *fd* excitation spectra for all rare earth ions in $CaF_2$ can be found in Ref. 15. The structure of the *fd* bands of the trivalent lanthanides was explained using a scheme of LS coupling and assuming that only electric dipole type transitions are allowed, but the *fd* bands could not be assigned unambiguously.

In a previous paper we have presented initial results on the fine structure in the *fd* excitation spectra for some light lanthanides in $LiYF_4$, together with energy-level calculations.[16] In this paper an extensive overview of the high-resolution *fd* excitation spectra of the light trivalent lan-

 

thanides ($Ce^{3+}$, $Pr^{3+}$, $Nd^{3+}$, $Sm^{3+}$, and $Eu^{3+}$) is presented. The rare-earth (RE) ions are incorporated in $LiYF_4$, $CaF_2$, or $YPO_4$ host lattices. In these lattices the ion-lattice coupling is relatively weak and fine structure (zero-phonon lines) of the *fd* bands can be expected. By recording excitation spectra using synchrotron radiation, high-resolution spectra in which the fine structure can be observed are obtained over the full energy range of interest (100–250 nm). Identification of the zero-phonon line gives exact information on the energy of the electronic transition and makes a comparison with energy level calculations possible. It is demonstrated that the energy levels and transition intensities of the $4f^n - 4f^{n-1}5d$ transitions for the light lanthanides can be quite satisfactorily explained by extension of the standard model used for energy-level calculations of $4f^n$ states.

## II. MODEL

For the calculations of the $4f^{n-1}5d$ energy levels the model for energy-level calculations within the $4f^n$ configuration is extended to calculate the energies of the $4f^{n-1}5d$ levels. The model is outlined in detail in Ref. 16. For the calculations the parameters for Coulomb interaction between the $4f$ electrons and spin-orbit interaction are needed, as well as the crystal-field interaction parameters for the $4f$ electrons. The values for these parameters have been determined for many lanthanide ions in various host lattices from fits of the experimentally observed positions of the $4f^n$ energy levels. For lanthanide ions in $LaF_3$ most extensive energy-level calculations have been reported, but also for lanthanides in the host lattices $LiYF_4$,[2] $YPO_4$,[18] and $CaF_2$,[19] which are investigated here, the parameters have been reported for many of the lanthanides. In addition to the $4f^n$ parameters, the energy-level calculations of $4f^{n-1}5d$ levels require crystal field and spin-orbit parameters for the $5d$ electron. These parameters can be obtained from fits of energy levels observed for $Ce^{3+}$. Finally, Coulomb interaction between the $4f$ electrons and the $5d$ electron has to be included. These *fd* interaction parameters can be obtained from *ab initio* calculations using standard computer programs for atoms. In addition to the splitting into many energy levels due to interactions within the $4f^{n-1}5d$ configuration, the position of the energy levels is determined by the energy difference between the bary center of the $4f^n$ ground configuration and the bary center of the $4f^{n-1}5d$ configuration $\Delta_E(fd)$. The influence of $\Delta_E(fd)$ is to shift all $4f^{n-1}5d$ energy levels by the same amount relative to the ground state and $\Delta_E(fd)$ is adjusted to obtain the best agreement between experiment and calculations.

In this paper we use $4f^n$ crystal field parameters[2,18,19] for the appropriate host lattice and $4f^n$ atomic parameters[17] calculated for the rare-earth ions in $LaF_3$. For $4f^{n-1}5d$ in $LiYF_4$, we use literature values for the $4f^n$ parameters for the same ion.[2] These parameters are not required to be identical for the $4f^n$ and $4f^{n-1}5d$ configuration but there is not enough information in the spectra to definitively test the effect of varying these parameters from the $4f^n$ values. For $4f^{n-1}5d$ in $YPO_4$, we used literature values for the $4f^n$ parameters for the $4f^{n-1}$ core.[18] For $4f^{n-1}5d$ in $CaF_2$, we used estimated values for the $4f^n$ parameters obtained from extrapolation of the literature values given for $Eu^{3+}$ (Ref. 19). For the *fd* interaction we used atomic (Coulomb and spin-orbit) parameters calculated from standard atomic computer programs.[20] The fitted parameters in our calculations are the $5d$ crystal-field parameters, which we obtained from fits of the $Ce^{3+}$ spectrum. These same crystal-field parameters are then used for the $Pr^{3+}$, $Nd^{3+}$, $Sm^{3+}$, and $Eu^{3+}$ calculations.

The *fd* transitions are dipole allowed and it is relatively easy to calculate the electric dipole matrix elements of $-erC_q^1$ for the transitions, where $C_q^1$ is a spherical tensor operator as defined in Refs. 20, 21. This is in contrast to transitions within the $4f^n$ configuration, for which a rather elaborate calculation is necessary, since admixing of other (opposite parity) states is required to make the transition allowed.[3] However, because the $5d$ orbitals are more spread out than the $4f$ orbitals, there is a displacement of the equilibrium positions of the ligands in the excited states and most intensity is in the vibronic bands.[22,23] In our modelling, we assume that the superposition of several vibrational modes gives rise to a Gaussian shape of the vibronic band. The energy-level calculations are performed for the zero-phonon line positions. To reproduce the experimentally observed spectra, Gaussian shaped bands are superimposed on the zero-phonon lines. The energy difference between the zero-phonon line origin and the maximum of the Gaussian vibronic band is estimated from the $Ce^{3+}$ spectra. This energy difference corresponds to half of the Stokes shift of the emission. Furthermore, we make the standard approximation that the intensities of the vibronic bands are proportional to the squares of the electric dipole moment operator evaluated between the initial and final electronic states.

## III. EXPERIMENT

### A. Sample preparation

$LiYF_4$ single crystals were prepared from LiF (15 mol % excess) and $YF_3$ ($4N$) in vitreous carbon crucibles using a Philips PH 1006/13 high frequency furnace. The crystal growth melt contained 1% $REF_3$ (RF=Ce, Pr, Nd, Sm, and Eu) unless mentioned otherwise (the maximal dopant concentration is 5%). The reactants were mixed and preheated over night at 300 °C in a nitrogen atmosphere. The crystal growth chamber was flushed with $SF_6$ as a reactive agent for half an hour while heating the sample from 550 to 750 °C, to remove traces of oxygen. At 750 °C the nitrogen flow was turned on and the sample was heated to the melting point (~900 °C). Then the sample was slowly cooled to room temperature. $LiYF_4$ has the inverse scheelite structure. The RE ion occupies the $Y^{3+}$ site ($S_4$).[24] Due to the small deviation from $D_{2d}$ symmetry, energy level calculations in $LiYF_4$ can be done by assuming a $D_{2d}$ crystal-field potential.

$CaF_2$ single crystals doped with 0.001% $RE^{3+}$ (RE=Ce, Pr, Nd, Sm) were prepared from $CaF_2$ and $REF_3$($3N$) following the same procedure as for $LiYF_4$ (melting temperature $CaF_2$ ~ 1300 °C). NaF was added as a charge compensator. In $CaF_2$ the trivalent RE ion is incorporated on a

divalent ($Ca^{2+}$) site and therefore charge compensation is required. The charge compensation can be provided by a local interstitial fluoride ion or by a distant fluoride interstitial, resulting in sites of $C_{4v}$ or $C_{3v}$ symmetry. It is also possible to add a charge compensator to the crystal growth melt. For example, addition of NaF will favor the formation of $O_h$ sites.[25] FTIR spectra of our crystals show that $O_h$ sites dominate. When other sites ($RE^{3+}$-$Na^+$ sites) were present, selective (V)UV excitation spectra could be performed to obtain information on one type of site only. At high dopant concentrations (>0.05%) cluster sites containing two or more RE ions will start to dominate. To avoid cluster sites, very low dopant concentrations (0.001%, unless mentioned otherwise) were used.

Crystalline powder samples of $YPO_4$ doped with 1% $RE^{3+}$ (RE=Ce, Pr, Nd, Sm, and Eu) were prepared by firing $Y_2O_3$(4N), $RE_2O_3$(4N), and $(NH_4)_2HPO_4$ in ambient atmosphere at 1350 °C for three hours. $YPO_4$ has the zircon structure, the lanthanide ion occupies the $Y^{3+}$ site which has $D_{2d}$ site symmetry.[26] The $LiYF_4$ and $YPO_4$ samples were analyzed with x-ray diffraction using a Philips PW1710 Diffractometer using Cu$K'_\alpha$ radiation (1.542 Å) and consisted of a single crystalline phase.

### B. Optical spectroscopy

Luminescence measurements in the VUV and UV part of the electromagnetic spectrum were performed at the HIGITI experimental station[27] of the DESY synchrotron in Hamburg, Germany. In excitation the spectral resolution was about 0.3 nm using a modified Wadsworth Mounting 1 m monochromator with a 1200 l/mm grating blazed at 150 nm. The excitation spectra were corrected for the spectral distribution of the synchrotron radiation intensity. Emission spectra in the VUV and UV spectral region were measured using a SEYA 0.2 m monochromator with a 1200 l/mm grating blazed at 150 nm and a Hamamatsu MCP 1645 U-09 channel plate detector. The typical resolution was 2 nm.

Excitation spectra for wavelengths longer than 250 nm were recorded on a SPEX 1680 spectrofluorometer, equiped with 0.22 m double monochromators blazed at 500 nm. The excitation source was a 450 W xenon lamp. The spectral resolution of this setup is about 0.5 nm. Excitation spectra measured on this apparatus were corrected for the spectral distribution of the lamp intensity by measuring the emission intensity from a rhodamine reference cell simultaneously. Emission spectra measured on this setup were corrected for the spectral response of the monochromator and the detector using typical correction spectra provided by the manufacturer. Measurements were performed at ~10 K using a cold finger cryostat.

## IV. RESULTS

### A. $Ce^{3+}$

For the understanding of the lanthanide *fd* structure, knowledge about the excitation spectrum of $Ce^{3+}$ in a certain host lattice is very important. The $Ce^{3+}$ ion has the $4f^1$ configuration, and irradiation with UV radiation will excite this

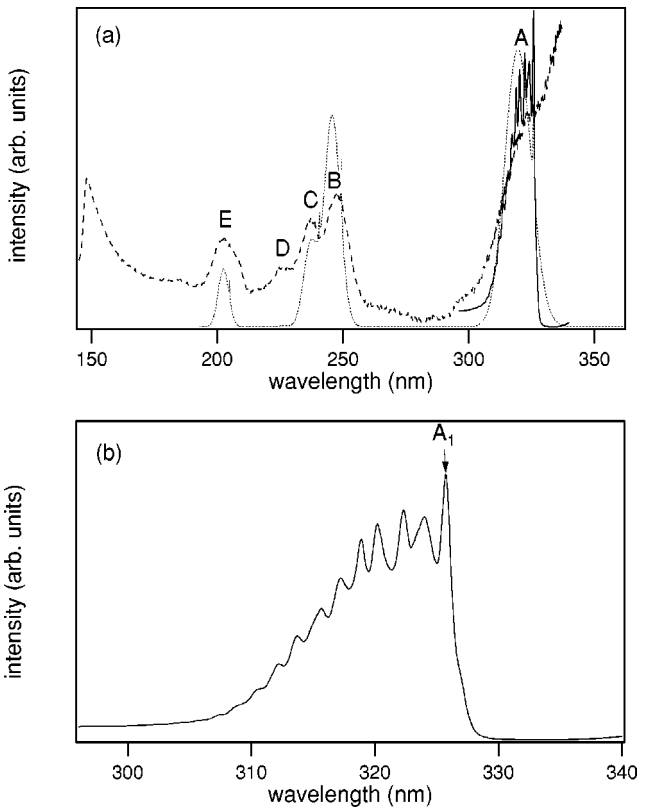


FIG. 1. Excitation spectrum of $YPO_4$ doped with 1% $Ce^{3+}$ recorded monitoring the $5d^1 \rightarrow {}^2F_{7/2}$ emission at 355 nm at 6 K. The broken line in (a) shows the excitation spectrum measured at DESY, the dotted line represents a fit using the $5d$ crystal field parameters as adjustable parameters. The solid line (a,b) is a higher resolution spectrum measured at the SPEX.

$4f$ electron into a $5d$ orbital, leaving the $4f$ shell empty. Therefore, the excitation spectrum of $Ce^{3+}$ will give direct information on the crystal-field splitting of the $5d$ orbitals. A similar crystal-field splitting is expected for all rare-earth ions in the same host lattice. The crystal-field splitting of the $5d$ states dominates the structure in the *fd* excitation spectra, even in the more complex (rare-earth ions with more than one $4f$ electron) cases.

#### *1. Experiment*

$YPO_4$. Figure 1 shows the excitation spectrum of the $Ce^{3+}$ emission in $YPO_4$:$Ce^{3+}$ 1% (broken and solid line). The excitation spectrum of $Ce^{3+}$ ($4f^1$) in the (V)UV part of the electromagnetic spectrum reflects the crystal-field splitting and spin-orbit coupling of the $5d$ electron. The spectrum shows four broad bands without structure with maxima at 248 nm (B), 237 nm (C), 227 nm (D), and 203 nm (E), and a structured band with a maximum at 323 nm (A). At 148 nm the host lattice starts to absorb.[28] The structured band at 323 nm is shown in more detail in Fig. 1(b) and consists of a zero-phonon line at 325.75 nm and a vibronic side band with a width [full width at half maximum (FWHM)] of 1100 $cm^{-1}$. The FWHM of the zero-phonon line is about 100 $cm^{-1}$, and is limited by the instrumental resolution. From the ratio of the intensity of the zero-phonon line to that of the

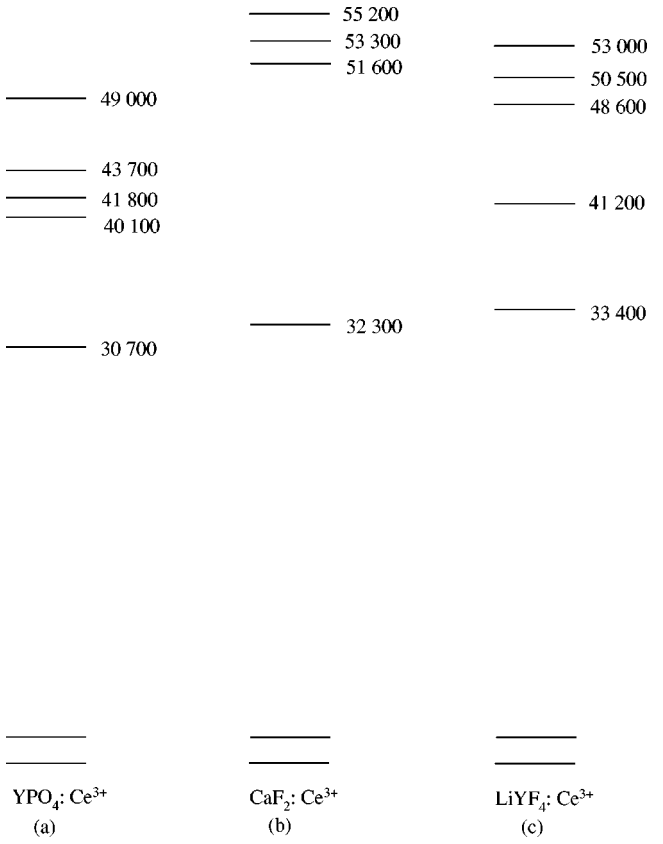


FIG. 2. Energy levels of $Ce^{3+}$ incorporated in $YPO_4$ (a), $CaF_2$ (b), and $LiYF_4$ (c). The position of the zero-phonon line is given. If no zero-phonon line was observed in the spectrum (for example for the transitions to the higher $5d$ crystal-field components), the electronic energy of the transition was obtained by subtracting an energy from the maximum of the vibronic band, equal to the displacement from the vibronic maximum to the electronic origin of the lowest energy $5d$ band.

whole structured band of about 0.125, the Huang-Rhys coupling constant ($S$) is determined to be 2 (intermediate coupling). The intensity distribution over the vibronic lines is consistent with an $S$ of about 2. The energy difference with the first vibronic lines is about 160 $cm^{-1}$. The overall pattern of the band cannot be reproduced by coupling to a single vibration, but could be reproduced by coupling to two vibrations of 160 and 350 $cm^{-1}$. The lines separated from $A_1$ by more than 350 $cm^{-1}$ are probably two or more-phonon lines.

The presently observed splitting of the $5d$ state for $Ce^{3+}$ in $YPO_4$ is very similar to the splitting for $Ce^{3+}$ in $LuPO_4$ [bands at 31 000, 39 800, 42 000, 44 500, and 50 500 $cm^{-1}$ (Ref. 29)] and agrees with the positions obtained from TPE for $YPO_4$:$Ce^{3+}$ in Ref. 30. The crystal field splitting for $Ce^{3+}$ in $YPO_4$ is slightly (some 1000 $cm^{-1}$) smaller than for $Ce^{3+}$ in $LuPO_4$, as expected for $Ce^{3+}$ on a larger cation site ($R_{Lu(III)}=0.97$ Å, $R_{Y(III)}=1.01$ Å in VIII coordination). Figure 2(a) shows the energy level scheme of $YPO_4$:$Ce^{3+}$. The lowest energy $fd$ aborption is observed at 30 698 $cm^{-1}$, which is 19 039 $cm^{-1}$ lower in energy than the position of the $5d$ state in the free ion.[31] Only for this band fine structure is observed. Excitation to the higher $5d$ crystal-field components gives structureless excitation bands. This situation is often encountered for $fd$ absorption and is explained by assuming that these high-energy $5d$ levels are located in the conduction band of the host lattice. If a $4f^{n-1}5d$ state is situated in the conduction band, resonant escape of an electron from the high-energy $4f^{n-1}5d$ state to the conduction band is possible. Especially for $Eu^{2+}$, $Yb^{2+}$, and $Ce^{3+}$ this process has been studied and confirmed by photoconductivity measurements.[32–36] Due to fast photoionization, the lifetime of the $4f^{n-1}5d$ states which are situated in the conduction band is very short. The short lifetime will result in line broadening (Heisenberg uncertainty principle: $\Delta E \Delta \tau \cong \hbar$) and sharp zero-phonon lines can no longer be observed.[37]

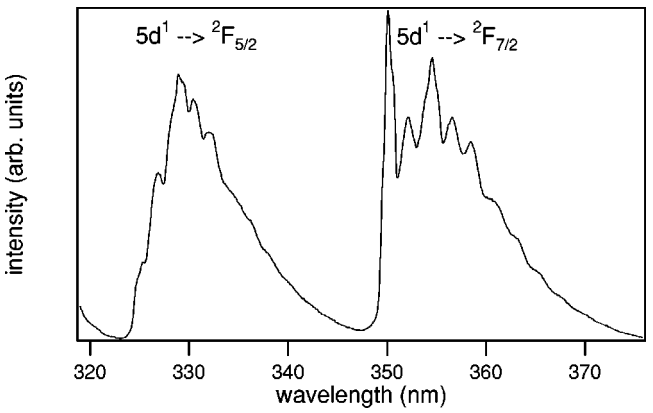


FIG. 3. Emission spectrum of $YPO_4$:$Ce^{3+}$ 1% at 6 K, recorded for excitation at 317 nm.

Figure 3 shows the emission spectrum of $YPO_4$:$Ce^{3+}$. Two structured bands are observed with maxima at 329 and 355 nm. The emission is due to transitions from the lowest $5d$ level to the $^2F_{5/2}$ and $^2F_{7/2}$ states of $Ce^{3+}$. The energy separation between the bands is 2190 $cm^{-1}$, in agreement with the separation between the $^2F_{5/2}$ and $^2F_{7/2}$ states of $Ce^{3+}$. The emission due to the transition to the $^2F_{7/2}$ excited state of $Ce^{3+}$ consists of a zero-phonon line and a vibronic side band with a width of 870 $cm^{-1}$. The crystal-field splitting of the $^2F_{7/2}$ level ($\sim$400 $cm^{-1}$) is not resolved. In the higher-energy emission band ($d \rightarrow {}^2F_{5/2}$) the zero-phonon line is weak, probably due to reabsorption. The Stokes shift (defined as the energy difference between the excitation maximum and emission maximum) is about 550 $cm^{-1}$ for the $fd$ transition of $Ce^{3+}$ in $YPO_4$.

$CaF_2$. The coordination of the RE ion in $CaF_2$ is a cubic eightfold coordination and therefore a splitting of the $5d$ orbitals in $^2E$ and $^2T_2$ is expected, $^2E$ being lower in energy, and the crystal-field splitting is expected to be large (crystal-field splitting in cubic eight coordination is about $\frac{8}{9}$ times the crystal field splitting in octahedral coordination). The $^2T_2$ state will be split further by spin-orbit coupling. Charge compensation is required when a trivalent lanthanide ion substitutes for a divalent Ca ion. In the case of charge compensation by $Na^+$, mainly cubic and $Na^+$ sites will be formed.

The excitation spectrum of the $Ce^{3+}$ emission in $CaF_2$ doped with 0.001% $Ce^{3+}$ is shown as the solid and broken lines in Fig. 4. Broad bands are observed with maxima at 306 nm (A) and 190 nm (B). The excitation band with a maxi-

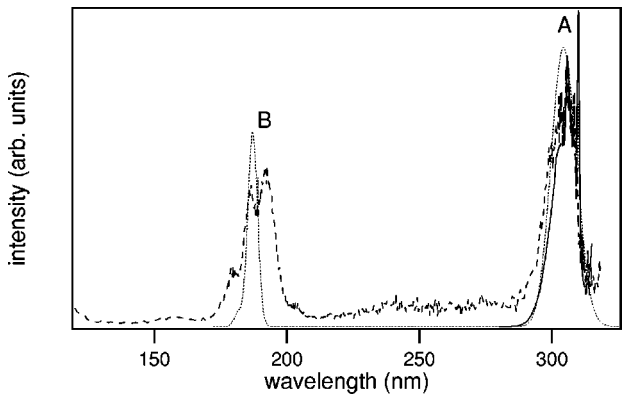


FIG. 4. Excitation spectrum of $CaF_2$ doped with 0.001% $Ce^{3+}$ recorded monitoring the $5d^1 \rightarrow {}^2F_{5/2}$ emission at 320 nm at 6 K. The broken line shows the excitation spectrum measured at DESY, the dotted line represents a fit using the $5d$ crystal-field parameters as adjustable parameters. The solid line is a higher resolution spectrum measured at the SPEX.

mum at 306 nm is assigned to the first *fd* transition on $Ce^{3+}$ $[4f^1 \rightarrow 5d^1({}^2E)]$. The excitation band with a maximum at 190 nm (band *B*) is assigned to the $4f^1 \rightarrow 5d^1({}^2T_2)$ transition and is split into three bands with maxima at 180, 186, and 192 nm. Note that the splitting is different than the splitting for uncompensated $CaF_2Ce^{3+}$ as observed by Manthey[38] due the different site symmetry. In Fig. 2(b) the $5d^1$ energy levels of $Ce^{3+}$ in $CaF_2$ are shown.

Detailed analysis shows that band A consists of a zero-phonon line at 309.9 nm ($A_1$) and a vibronic side band with a width of about 1500 $cm^{-1}$. The zero-phonon line $A_1$ is observed at a slightly longer wavelength than the value reported in the literature for the zero-phonon *fd* transition of $Ce^{3+}$ on a cubic site in $CaF_2$ (309.25 nm).[25] This is probably due to an error in the wavelength calibration of about 0.8 nm. The energy separation between zero-phonon line $A_1$ and phonon line $A_1'$ is about 430 $cm^{-1}$ and may be explained in terms of phonon frequencies corresponding to local modes involving the $Ce^{3+}$ ion and its nearest neighbors, such as the local breathing mode oscillations of the eight fluoride ions surrounding the RE ion. The FWHM of the zero-phonon line is about 130 $cm^{-1}$ and is determined by the resolution of the experimental setup. The ratio of the intensity of the zero-phonon line to that of the whole structured band is about 0.085, corresponding to a Huang-Rhys factor of 2.5 (intermediate coupling). The ion-lattice coupling seems to be larger in $CaF_2$ than in $YPO_4$, which is also reflected in the less resolved fine structure pattern in $CaF_2$ compared to $YPO_4$. In addition to the 430 $cm^{-1}$ vibration, a phonon frequency of about 145 $cm^{-1}$ can be observed in the excitation spectrum. This frequency is slightly larger than the vibronic frequency observed for $Pr^{3+}$ and $Nd^{3+}$ ($\sim$142 $cm^{-1}$) (Ref. 39) and agrees with the trend that the phonon frequency decreases for the heavier lanthanides due to their increasing mass.[39]

In the emission spectrum of $CaF_2$:$Ce^{3+}$ 0.001% (Fig. 5) bands are observed at 315 and 338 nm due to the transitions from the lowest $5d$ state to the ${}^2F_{5/2}$ and ${}^2F_{7/2}$ levels. The emission bands consist of a zero-phonon line and a vibrational side band (width about 1100 $cm^{-1}$). The energy separation between *B* and *B'* is 430 $cm^{-1}$, the same vibronic energy as observed in the excitation spectrum. The Stokes shift for the *fd* transition of $Ce^{3+}$ in $CaF_2$ is about 900 $cm^{-1}$, somewhat larger than in $YPO_4$ in agreement with the larger ion-lattice coupling for $CaF_2$.

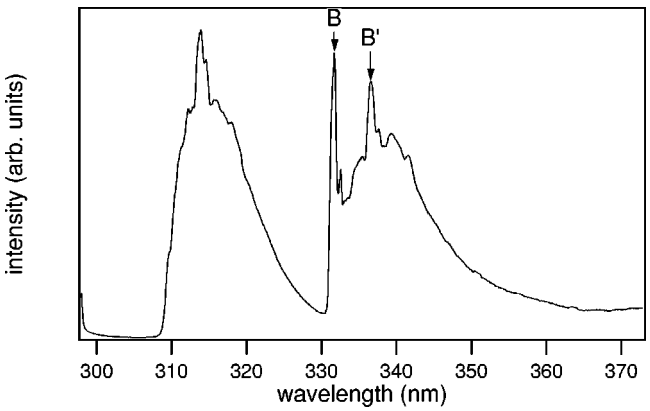


FIG. 5. Emission spectrum of $CaF_2$:$Ce^{3+}$ 0.001% at 6 K, recorded for excitation at 295 nm.

$LiYF_4$. In $LiYF_4$ the rare-earth ion occupies a site of $S_4$ symmetry. The site symmetry is close to $D_{2d}$ and can be interpreted as a distortion of a cubic field which splits the *E* and $T_2$ states. Figure 6 (solid line) shows the excitation spectrum of powdered $LiYF_4$ doped with 1% $Ce^{3+}$. Broad bands are observed with maxima at 294 nm (A), 240 nm (B), 203 nm (C), 196 nm (D), and 187 nm (E) due to transitions from the $Ce^{3+}$ ${}^2F_{5/2}$ ground state to the various $5d$ crystal field components. This observation is in agreement with the results of Combes *et al.*[40] The low intensity band at 219 nm is not assigned and may be due to an impurity. In Fig. 2(c) the energy levels of the excited $4f^0 5d^1$ configuration of $Ce^{3+}$ in $LiYF_4$ are presented.

Again the first *fd* transition consists of a zero-phonon line (at 299.11 nm) and a vibronic side band (FWHM$\sim$1940 $cm^{-1}$). The vibronic structure of this band is not well re-

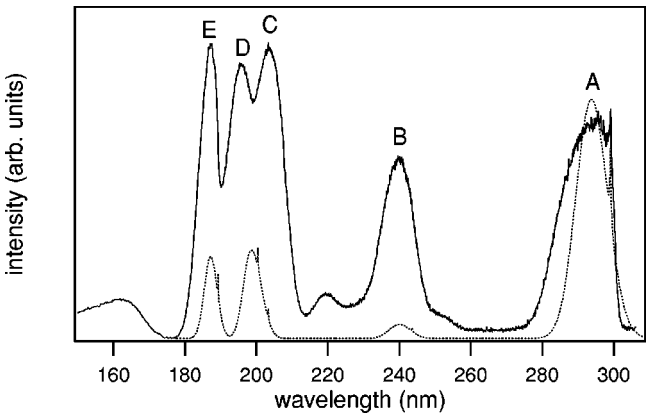


FIG. 6. Excitation spectrum of $LiYF_4$ doped with 1% $Ce^{3+}$ recorded monitoring the $5d^1 \rightarrow {}^2F_{7/2}$ emission at 327 nm at 6 K. The solid line shows the excitation spectrum measured at DESY, the dotted line represents a fit using the $5d$ crystal-field parameters as adjustable parameters.

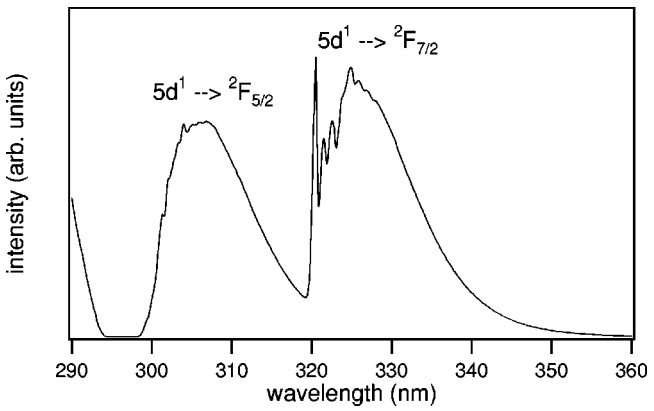


FIG. 7. Emission spectrum of $LiYF_4$:$Ce^{3+}$ 1% at 6 K, recorded for excitation at 280 nm.

solved. The electronic origins for the other transitions are not observed and are thought to be broadened by photoionization to the conduction band and therefore unobservable.[36,37] The FWHM of the *fd* excitation bands is about 2000 $cm^{-1}$ and the maximum of the first band is offset from the electronic origin by about 600 $cm^{-1}$.

In the emission spectrum of $LiYF_4$:$Ce^{3+}$ 1% excited at 280 nm two broad bands are observed with maxima at 306 and 325 due to the transitions from the lowest $5d$ state to the $^2F_{5/2}$ and $^2F_{7/2}$ levels (see Fig. 7). The emission bands consist of a zero-phonon line and a vibronic side band (width about 1000 $cm^{-1}$). In the higher-energy emission band ($d \rightarrow {}^2F_{5/2}$) the zero-phonon line is weak, probably due to reabsorption. The Stokes shift for the *fd* transition of $Ce^{3+}$ in $LiYF_4$ is about 1300 $cm^{-1}$, which is larger than in $YPO_4$ and $CaF_2$ and might explain the less resolved fine structure pattern in $LiYF_4$.

### *2. Model*

The excitation spectra of the $Ce^{3+}$ emission in $YPO_4$, $CaF_2$, and $LiYF_4$ doped with $Ce^{3+}$ give information on the splitting of the $5d$ state due to the crystal-field and spin-orbit coupling. This information is needed for the interpretation of the *fd* excitation spectra of the other rare-earth ions in the same host lattices where, in addition to the splitting of the $5d$ state, interaction within the $f^{n-1}$ core and interaction between $f^{n-1}$ and $5d$ give rise to additional structure. In Fig. 2 the splitting for the $5d$ state, as observed in $YPO_4$, $CaF_2$, and $LiYF_4$, is shown. In all cases the positions of the zero-phonon lines are given. When no zero-phonon line was observed (for example for the transitions to the higher $5d$ crystal field components), the electronic energy of the transition was obtained by subtracting an energy from the maximum of the vibronic band, equal to the displacement from the vibronic maximum of the electronic origin of the first $5d$ band. To try to calculate the observed splitting, the spin-orbit parameter was fixed to a value known from the literature[30,20] (see Table II) and the energy levels were fitted allowing the crystal field parameters to vary. This gave the calculated results shown in Table I and the parameters presented in Table II. The fitted $5d$ crystal-field parameters have the same signs as the $4f$ parameters, but are about twenty times larger, which is expected, since the $5d$ orbitals are much more extended than the (shielded) $4f$ orbitals.

TABLE I. Observed and calculated energies for the $5d$ states of $Ce^{3+}$ in $YPO_4$, $CaF_2$, and $LiYF_4$, in $cm^{-1}$. The energies given here are for the electronic origins. For the lowest-energy $5d$ state the position of the experimentally observed zero-phonon line is given. For the higher-energy $5d$ states the positions of the zero-phonon lines given in this table have been estimated by subtracting 400 $cm^{-1}$ (for $LiYF_4$ and $CaF_2$) or 300 $cm^{-1}$ (for $YPO_4$) from the position of the maximum of the vibronic band. Irreducible representations for cubic and $D_{2d}$ symmetry are given.

| | Exp. | Calc. | Cubic parentage | $D_{2d}$ | Cubic |
|---|---|---|---|---|---|
| $YPO_4$ | 30698 | 30701 | $^2E$ | $\Gamma_7$ | |
| | 40058 | 40095 | $^2E$ | $\Gamma_6$ | |
| | 41929 | 41562 | $^2T_2$ | $\Gamma_7$ | |
| | 43788 | 43668 | $^2T_2$ | $\Gamma_6$ | |
| | 48996 | 48814 | $^2T_2$ | $\Gamma_7$ | |
| $CaF_2$ | 32300 | 32267 | $^2E$ | | $\Gamma_8$ |
| | 51600 | 52857 | $^2T_2$ | | $\Gamma_8$ |
| | 53300 | 52857 | $^2T_2$ | | $\Gamma_8$ |
| | 55200 | 54395 | $^2T_2$ | | $\Gamma_7$ |
| $LiYF_4$ | 33433 | 33433 | $^2E$ | $\Gamma_7$ | |
| | 41101 | 41062 | $^2E$ | $\Gamma_6$ | |
| | 48564 | 49179 | $^2T_2$ | $\Gamma_6$ | |
| | 50499 | 49888 | $^2T_2$ | $\Gamma_7$ | |
| | 52790 | 52815 | $^2T_2$ | $\Gamma_7$ | |

The fits are shown as the dotted lines in Figs. 1, 4, and 6. For $YPO_4$ the fitted spectrum agrees well with the experimental spectrum. However, the calculated intensity of the transition to the fourth $5d$ crystal field component is about 100 times lower than the other transitions and is therefore not observed in the calculated spectrum. The fact that this band is observed in the experimental spectrum may be due to some mixing of *d* states, which lifts the selection rule. The presently found crystal-field parameters to explain the structure in the *d* excitation spectrum of $Ce^{3+}$ in $YPO_4$ differ from the values for $LuPO_4$:$Ce^{3+}$ in Ref. 30. In this article the value for the spin-orbit coupling $\zeta$ was an adjustable parameter and the best fit was obtained for a very small value for $\zeta$. In this paper we have kept the spin-orbit parameter fixed at the value calculated for $Ce^{3+}$ in $LuPO_4$, recently crystal-field parameters were reported for the splitting of the $5d$ state for $Pr^{3+}$ in $YPO_4$, based on excited state absorption spectra.[41] The parameters reported in Ref. 41 differ from the presently reported parameters. The origin of the difference is not clear.

For $CaF_2$ the experimental spectrum is not completely reproduced at high energies. The crystal field splits the $5d$ orbitals into two sets $^2E$ and $^2T_2$, $^2E$ being lower in energy. The $^2T_2$ orbitals are split in two components by spin-orbit coupling, which is also observed in the experimental spectrum as the bands with maxima at 180 and 186 nm. However, the presence of a third band is not explained by the theory.

The calculated spectrum of $LiYF_4$ agrees fairly well with the experimental spectrum. The fit in the high-energy region

TABLE II. Parameters used for energy level calculations for $4f^n$ and $4f^{n-1}5d$ configurations of $Ce^{3+}$, $Pr^{3+}$, $Nd^{3+}$, $Sm^{3+}$, and $Eu^{3+}$ in $YPO_4$, $CaF_2$, and $LiYF_4$. Parameters for the splitting of the $4f^{n-1}$ core (such as parameters for Coulomb interaction, spin-orbit interaction, and crystal-field splitting) are obtained from literature.[2,17–19] The $fd$ interaction parameters are calculated using Cowan's code (Ref. 20) and for the crystal-field splitting of the $5d$ state, parameters are obtained from the fits of the $Ce^{3+}$ spectra. Further details are provided in the text. Units are in $cm^{-1}$.

| | Ce | | | Pr | | | Nd | | | Sm | Eu |
|---|---|---|---|---|---|---|---|---|---|---|---|
| | $YPO_4$ | $CaF_2$ | $LiYF_4$ | $YPO_4$ | $CaF_2$ | $LiYF_4$ | $YPO_4$ | $CaF_2$ | $LiYF_4$ | $LiYF_4$ | $LiYF_4$ |
| $F^2(ff)$ | | | | 68878 (Ref. 17) | 68878 (Ref. 17) | 68878 (Ref. 17) | 73018 (Ref. 17) | 73018 (Ref. 17) | 73018 (Ref. 17) | 79805 (Ref. 17) | 83125 (Ref. 17) |
| $F^4(ff)$ | | | | 50347 (Ref. 17) | 50347 (Ref. 17) | 50347 (Ref. 17) | 52789 (Ref. 17) | 52789 (Ref. 17) | 52789 (Ref. 17) | 57175 (Ref. 17) | 59268 (Ref. 17) |
| $F^6(ff)$ | | | | 32901 (Ref. 17) | 32901 (Ref. 17) | 32901 (Ref. 17) | 35757 (Ref. 17) | 35757 (Ref. 17) | 35757 (Ref. 17) | 40250 (Ref. 17) | 42560 (Ref. 17) |
| $\alpha(ff)$ | | | | 16.23 (Ref. 17) | 16.23 (Ref. 17) | 16.23 (Ref. 17) | 21.34 (Ref. 17) | 21.34 (Ref. 17) | 21.34 (Ref. 17) | 20.16 (Ref. 17) | 20.16 (Ref. 17) |
| $\beta(ff)$ | | | | −566.6 (Ref. 17) | −566.6 (Ref. 17) | −566.6 (Ref. 17) | −593 (Ref. 17) | −593 (Ref. 17) | −593 (Ref. 17) | −566 (Ref. 17) | −566 (Ref. 17) |
| $\gamma(ff)$ | | | | 1371 (Ref. 17) | 1371 (Ref. 17) | 1371 (Ref. 17) | 1445 (Ref. 17) | 1445 (Ref. 17) | 1445 (Ref. 17) | 1500 (Ref. 17) | 1500 (Ref. 17) |
| $T_2(ff)$ | | | | | | | 298 (Ref. 17) | 298 (Ref. 17) | 298 (Ref. 17) | 300 (Ref. 17) | 300 (Ref. 17) |
| $T_3(ff)$ | | | | | | | 35 (Ref. 17) | 35 (Ref. 17) | 35 (Ref. 17) | 36 (Ref. 17) | 40 (Ref. 17) |
| $T_4(ff)$ | | | | | | | 59 (Ref. 17) | 59 (Ref. 17) | 59 (Ref. 17) | 56 (Ref. 17) | 60 (Ref. 17) |
| $T_6(ff)$ | | | | | | | −285 (Ref. 17) | −285 (Ref. 17) | −285 (Ref. 17) | −347 (Ref. 17) | −300 (Ref. 17) |
| $T_7(ff)$ | | | | | | | 332 (Ref. 17) | 332 (Ref. 17) | 332 (Ref. 17) | 373 (Ref. 17) | 370 (Ref. 17) |
| $T_8(ff)$ | | | | | | | 305 (Ref. 17) | 305 (Ref. 17) | 305 (Ref. 17) | 348 (Ref. 17) | 320 (Ref. 17) |
| $\zeta(ff)$ | 614.9 (Ref. 18) | 614.9 (Ref. 18) | 614.9 (Ref. 18) | 744 (Ref. 18) | 751.7 (Ref. 17) | 751.7 (Ref. 17) | 878 (Ref. 18) | 885.3 (Ref. 17) | 885.3 (Ref. 17) | 1176 (Ref. 17) | 1338 (Ref. 17) |
| $M_0(ff)$[a] | | | | 2.08 (Ref. 17) | 2.08 (Ref. 17) | 2.08 (Ref. 17) | 2.11 (Ref. 17) | 2.11 (Ref. 17) | 2.11 (Ref. 17) | 2.60 (Ref. 17) | 2.10 (Ref. 17) |
| $P_2(ff)$[b] | | | | −88.6 (Ref. 17) | −88.6 (Ref. 17) | −88.6 (Ref. 17) | 192 (Ref. 17) | 192 (Ref. 17) | 192 (Ref. 17) | 357 (Ref. 17) | 360 (Ref. 17) |
| $B20(ff)$ | 26 (Ref. 18) | | 481 (Ref. 2) | 26 (Ref. 18) | | 481 (Ref. 2) | 21 (Ref. 18) | | 409 (Ref. 2) | 348 (Ref. 2) | 348 (Ref. 2) |
| $B40(ff)$ | 263 (Ref. 18) | −1900 (Ref. 19) | −1150 (Ref. 2) | 263 (Ref. 18) | −1900 (Ref. 19) | −1150 (Ref. 2) | 280 (Ref. 18) | −1900 (Ref. 19) | −1135 (Ref. 2) | −775 (Ref. 2) | −775 (Ref. 2) |
| $B44(ff)$ | −1247 (Ref. 18) | −1135 (Ref. 19) | −1228 (Ref. 2) | −1247 (Ref. 18) | −1135 (Ref. 19) | −1228 (Ref. 2) | −808 (Ref. 18) | −1135 (Ref. 19) | −1216 (Ref. 2) | −1045 (Ref. 2) | −1045 (Ref. 2) |
| $B60(ff)$ | −1270 (Ref. 18) | 500 (Ref. 19) | −89 (Ref. 2) | −1270 (Ref. 18) | 500 (Ref. 19) | −89 (Ref. 2) | −1658 (Ref. 18) | 500 (Ref. 19) | 27 (Ref. 2) | −80 (Ref. 2) | −80 (Ref. 2) |
| $B64(ff)$ | 148 (Ref. 18) | −935 (Ref. 19) | −1213 (Ref. 2) | 148 (Ref. 18) | 935 (Ref. 19) | −1213 (Ref. 2) | 291 (Ref. 18) | 935 (Ref. 19) | −1083 (Ref. 2) | −772 (Ref. 2) | −772 (Ref. 2) |
| $\Delta_E(fd)$ | 39488 | 43516 | 43754 | 47516 | 52760 | 51690 | 53500 | 57043 | 57849 | 68238 | 73057 |
| $F^2(fd)$ | | | | 30271 (Ref. 20) | 30271 (Ref. 20) | 30271 (Ref. 20) | 30300 (Ref. 20) | 30300 (Ref. 20) | 30300 (Ref. 20) | 30300 (Ref. 20) | 30300 (Ref. 20) |
| $F^4(fd)$ | | | | 15094 (Ref. 20) | 15094 (Ref. 20) | 15094 (Ref. 20) | 15038 (Ref. 20) | 15038 (Ref. 20) | 15038 (Ref. 20) | 15038 (Ref. 20) | 15038 (Ref. 20) |
| $G^1(fd)$ | | | | 12903 (Ref. 20) | 12903 (Ref. 20) | 12903 (Ref. 20) | 12914 (Ref. 20) | 12914 (Ref. 20) | 12914 (Ref. 20) | 12914 (Ref. 20) | 12914 (Ref. 20) |
| $G^3(fd)$ | | | | 11160 (Ref. 20) | 11160 (Ref. 20) | 11160 (Ref. 20) | 11135 (Ref. 20) | 11135 (Ref. 20) | 11135 (Ref. 20) | 11135 (Ref. 20) | 11135 (Ref. 20) |
| $G^5(fd)$ | | | | 8691 (Ref. 20) | 8691 (Ref. 20) | 8691 (Ref. 20) | 8659 (Ref. 20) | 8659 (Ref. 20) | 8659 (Ref. 20) | 8659 (Ref. 20) | 8659 (Ref. 20) |
| $\zeta(dd)$ | 995.6 (Ref. 30) | 1082 (Ref. 20) | 1082 (Ref. 20) | 1149 (Ref. 20) | 1149 (Ref. 20) | 1149 (Ref. 20) | 1216 (Ref. 20) | 1216 (Ref. 20) | 1216 (Ref. 20) | 1351 (Ref. 20) | 1419 (Ref. 20) |
| $B20(dd)$ | 4756 | | 4673 | 4756 | | 4673 | 4756 | | 4673 | 4673 | 4673 |
| $B40(dd)$ | 3010 | −44016 | −18649 | 3010 | −44016 | −18649 | 3010 | −44016 | −18649 | −18649 | −18649 |
| $B44(dd)$ | −22452 | −26305 | −23871 | −22452 | −26905 | −23871 | −22452 | −26305 | −23871 | −23871 | −23871 |

[a] $M2$ and $M^4$ parameters were included with the ratios $M^2/M^0 = 0.56$ and $M^4/M^0 = 0.31$.
[b] $P^4$ and $P^6$ parameters were included with the ratios $P^4/P^2 = 0.5$ and $P^6/P^2 = 0.1$.

has improved in comparison with the fit presented in our previous publication.[16] By changing the assignment of the three high-energy $5d$ levels a better fit for $Ce^{3+}$ and also for the other lanthanides is obtained. The parameters used in this paper are more consistent with the parameters used in calculations for $LiYF_4:Pr^{3+}$ (Ref. 43). For this system polarization-dependent measurements were performed, allowing detailed comparison of the experimental and calculated energy levels. The intensities measured for the lowest two transitions in our spectrum is not accurate. In this energy region large corrections to the experimental spectrum had to be made due to the low synchrotron intensity for wavelengths longer than 230 nm. The agreement with the intensity ratio in the excitation spectrum of $LiYF_4:Ce^{3+}$ reported in Ref. 40 is better. The splitting of the two highest-energy states is still not very well reproduced. This problem has been discussed previously and is thought to be a result of relaxation of the ligands in the excited state, which lowers the symmetry.[42] In Table II the parameters used to fit the positions of the experimentally observed *fd* excitation bands are given. The $5d$ crystal-field parameters are used to calculate the splitting of the $5d$ state in case of the *fd* energy-level calculations. The actual crystal-field splitting may decrease slightly for the heavier (and smaller) lanthanide ions. Comparison of the crystal-field splitting observed for $Ce^{3+}$ and $Tb^{3+}$ (Ref. 44) in the same host lattice shows a decrease in the crystal-field splitting of about 5%.

### B. $Pr^{3+}$

#### *1. Experiment*

$YPO_4$. Figure 8 (solid line) shows the excitation spectrum of the $Pr^{3+}$ emission for $YPO_4$ doped with 1% $Pr^{3+}$. The bands with maxima at 227 nm (A), 187 nm (C), 176 nm (D), and 160 nm (E) correspond to transitions to, respectively, the first, second, fourth, and fifth $5d$ crystal-field component, as is clear from comparison with the excitation spectrum of $Ce^{3+}$ in $YPO_4$. The transition to the third $5d$ level is expected at 181 nm and is not observed as a separate band in the spectrum. This excitation band is probably located under the second and fourth *fd* band. Host lattice absorption starts at 148 nm. In the excitation spectrum the onset of the host lattice absorption is observed as a steep decrease. Since host lattice absorption is a competing absorption which does not result in the emission that is monitored (due to inefficient energy transfer from the host lattice to the emitting state of $Pr^{3+}$) the signal decreases for wavelengths shorter than 148 nm. The excitation band with a maximum at 195 nm (B) has a sharp onset. This might be due to the direct excitation of a $4f$ electron to the conduction band edge (photoionization onset). From the onset, the position of the $^3H_4$ ground state in the bandgap can be estimated to be about 50 000 $cm^{-1}$ below the conduction band. Further measurements (photoconductivity) should confirm this.

The lowest-energy *fd* excitation band is plotted in more detail in Fig. 8(b). It has a rich vibronic structure. The lowest-energy zero-phonon line ($A_1$) is observed at 229.75 nm. The assignment of higher-energy lines is difficult. This is because the interactions between the $4f$ electron and the

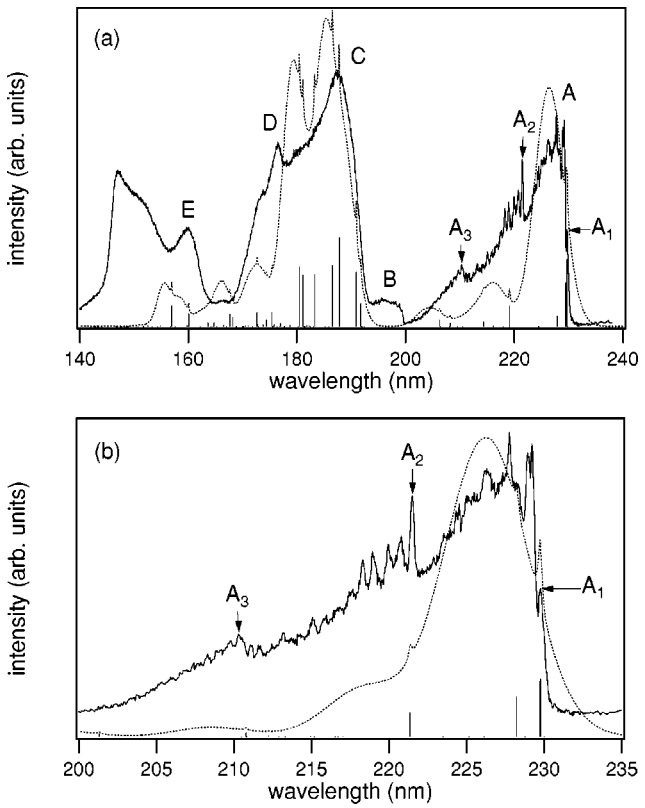


FIG. 8. Excitation spectrum of $YPO_4$ doped with 1% $Pr^{3+}$ at 6 K, recorded monitoring the $4f^15d^1 \rightarrow {}^3H_5$ emission at 247 nm. The solid line in (a) shows the excitation spectrum measured at DESY, the dotted line represents the calculated spectrum. Positions of the calculated electronic states are indicated in the spectrum by sticks to the horizontal axis. (b) shows the transition to the first $5d$ crystal-field component in more detail. Again, the dotted line represents the calculated spectrum, but this time *fd* parameters of 50% of the calculated value were used to improve the fit.

$5d$ electron in the $Pr^{3+}$ ion will give rise to many *fd* energy levels in addition to vibronic lines. The distinction between phonon associated lines and no-phonon lines is difficult.

The lowest *fd* excitation band seems to be split in three parts. A second region of sharp lines starts with a zero-phonon line ($A_2$) at 221.48 nm, separated from $A_1$ by 1625 $cm^{-1}$. The fine structure pattern of this second band is different from the first one. A number of regularly spaced vibronic lines, approximately 160 $cm^{-1}$ apart, can be observed. The vibronic frequency of 160 $cm^{-1}$ is in agreement with the vibrational frequency observed from recent ESA measurements for $YPO_4:Pr^{3+}$ (Ref. 41). A third region of lines starts at 210.3 nm, indicated by $A_3$ in Fig. 8(b), and is separated by 4025 $cm^{-1}$ from $A_1$.

It is not possible to explain the structure of the first *fd* excitation band by the assumption that the lowest level of the crystal-field split $5d$ state is coupled to the spin-orbit and crystal-field split $4f^1$ core. The distance between two no-phonon lines $A_1$ and $A_2$ is 1625 $cm^{-1}$, 75% of the splitting between the $Ce^{3+}$ $^2F_{7/2}$ and $^2F_{5/2}$ level. Although this is not very different from the 2000 $cm^{-1}$ usually observed for the $4f^1$ core, the presence of a third band at some 4000 $cm^{-1}$

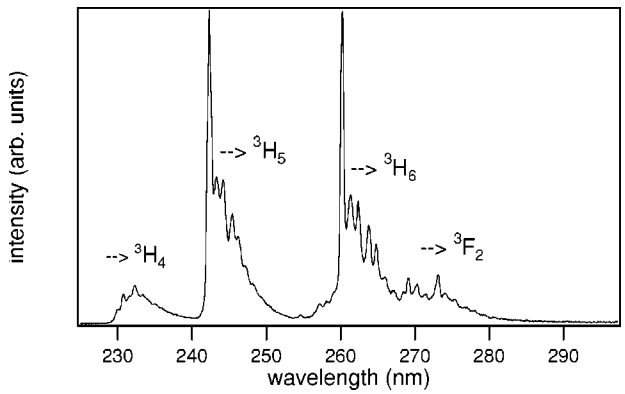


FIG. 9. UV emission spectrum of $YPO_4$:$Pr^{3+}$ 1%, recorded for excitation at 189 nm at 6 K.

cannot be explained using this simple model. A similar splitting into three bands is also observed in the other host lattices (see below).

The transition to the second crystal-field component (band C) also seems to be split. A shoulder at 173 nm is separated by 4200 $cm^{-1}$ from the maximum of the transition to the second $5d$ level at 187 nm, similar to the splitting of the first *fd* band (4025 $cm^{-1}$).

Figure 9 shows the (uncorrected) emission spectrum of $YPO_4$:$Pr^{3+}$ in the UV region. Emission from the lowest *fd* level to the $4f^2$ states of $Pr^{3+}$ is observed. Transitions from the lowest $4f^15d$ state to the $^3H_4$, $^3H_5$, and $^3H_6$ multiplets are indicated in Fig. 9. The emission spectrum is in agreement with the x-ray excited luminescence spectrum of Ref. 45, but in our spectrum fine structure (zero-phonon lines and vibronic lines) is observed. The zero-phonon line of the transition to the $^3H_4$ ground state is weaker due to reabsorption. At least two vibrations seem to be involved in the emission process. Evidence for coupling with a vibration of about 160 and about 315 $cm^{-1}$ can be found in the $Pr^{3+}$ emission spectrum.

$CaF_2$. In Fig. 10 the excitation spectrum of the $Pr^{3+}$ emission in $CaF_2$ doped with 0.001% $Pr^{3+}$ is shown. Two bands can be observed with maxima at 218 (A) and 154 nm (B), which can be assigned to transitions of a $Pr^{3+}$ $4f$ electron to the $^2E$ and $^2T_2$ levels. The excitation spectrum shown in Fig. 10 is different from the absorption spectrum reported in the literature,[15] especially in the spectral region between 160 and 195 nm, where strong absorptions were reported. This difference might be due to the higher $Pr^{3+}$ concentration used in Ref. 15. At higher concentration cluster sites form which have a lower site symmetry and *fd* bands between 160–195 nm can be expected. In an absorption spectrum all sites will be observed. In an excitation spectrum a single type of site can be selectively measured by choosing a proper emission wavelength. The first *fd* excitation band has a well resolved fine structure. The positions of three zero-phonon lines are indicated, located at 223.48 nm ($A_1$), 213.78 nm ($A_2$), and 202.83 nm ($A_3$). Vibronic side bands are at about 130 and 420 $cm^{-1}$ from the zero-phonon lines. The vibronic replica at 420 $cm^{-1}$ from the electronic origin is labeled $A_1'$ and probably corresponds to the Pr-*F* breathing mode. The zero-phonon line at 223.48 nm is located at about 400 $cm^{-1}$ lower energy than the zero-phonon line reported for $Pr^{3+}$ on a $C_{4v}$ site (221.5 nm).[46] In Ref. 15 the zero-phonon line at 223.48 nm was also observed in the absorption spectrum of a $CaF_2$ crystal doped with 0.05% $Pr^{3+}$, but this line disappeared upon decreasing the dopant concentration to 0.001%. Therefore this no-phonon line was thought to be due to an *fd* transition of cluster sites in the lattice. However, we do observe this transition in $CaF_2$ crystals doped with the same low $Pr^{3+}$ concentration (0.001%), in which the presence of clusters is not very probable. Further details on the nature of the different sites in $CaF_2$:$Pr^{3+}$ will be published in Ref. 46.

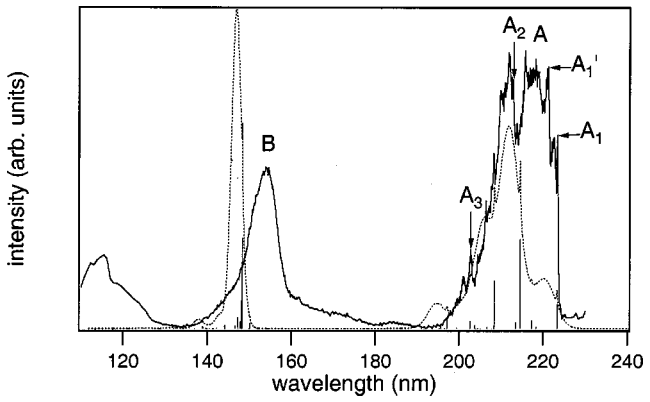


FIG. 10. Excitation spectrum of $CaF_2$:$Pr^{3+}$, $Na^+$ 0.001% at 6 K, recorded monitoring the $4f^15d^1 \rightarrow {}^3F_2$ emission at 265 nm.

Just as in $YPO_4$, the lowest *fd* excitation band is split into three bands. The energy difference between the levels in $CaF_2$ can be determined exactly, because fine structure is observed. The energy separation between the no-phonon lines $A_1$ and $A_2$ is 2030 $cm^{-1}$, the energy difference between $A_1$ and $A_3$ is 4556 $cm^{-1}$. This is similar to the splitting observed in $YPO_4$.

$LiYF_4$. Figure 11 (solid line) shows the excitation spectrum of the $Pr^{3+}$ emission in $LiYF_4$ doped with 2% $Pr^{3+}$. At 214 nm (A), 185 nm (B), 161 nm (C), and 149 nm (D), transitions from the $^3H_4$ level of $Pr^{3+}$ to the first, second, third and fifth crystal field component of the $4f5d$ configuration can be observed. The transition to the fourth $5d$ crystal-field component is obscured by the excitation bands corresponding to transitions to the third and fifth $5d$ level. The excitation bands observed at higher energy are probably due to $4f \rightarrow 6s$ or charge transfer (CT) transitions. No fine structure is observed in the excitation spectrum of $Pr^{3+}$ in $LiYF_4$.

The lowest *fd* excitation band is split into three bands. The energy separation between the maximum of the first and second band is about 1450 $cm^{-1}$, the separation between the first and the third band is about 3660 $cm^{-1}$. Also the transition to the second $5d$ crystal-field component seems to be split, the energy differences between the bands are about 1200 and about 3630 $cm^{-1}$, respectively. This splitting is similar to the splitting observed for the $4f^15d$ excited state of $Pr^{3+}$ in $YPO_4$ and $CaF_2$. It is clearly not the splitting in two bands separated by 2000 $cm^{-1}$ expected in the absence of *f-d* coupling. In the following section calculations will be

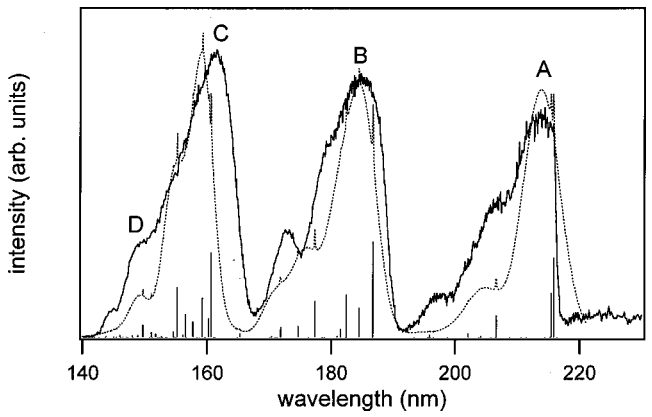


FIG. 11. Excitation spectrum of $LiYF_4:Pr^{3+}$ 2% at 6 K, recorded monitoring the $^3P_0 \rightarrow {}^3H_4$ emission at 480 nm.

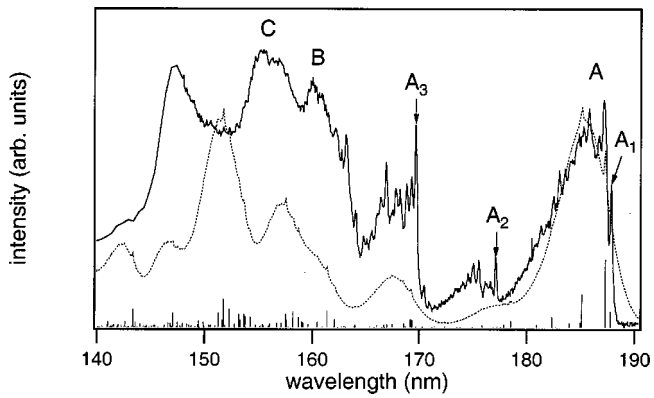


FIG. 12. Excitation spectrum of $YPO_4$ doped with 1% $Nd^{3+}$ at 6 K, recorded monitoring the $4f^2 5d^1 \rightarrow {}^4I_j$ emission at 197 nm.

presented to explain the structure observed in the excitation spectra.

#### *2. Model*

To explain the structure observed in the $4f^1 5d$ excitation spectra of $Pr^{3+}$ in $YPO_4$, $CaF_2$, and $LiYF_4$, energy level simulations as outlined in Sec. II were performed. The parameters used in the calculations are tabulated in Table II.

The calculated spectra are shown as the dotted lines in Figs. 8(a), 10, and 11. The calculated spectra match the experimental results quite well. The theory explains the splitting of the $5d$ crystal-field components into several bands. The calculated intensity of the transitions to the several crystal-field components agrees with the experimentally observed values. The intensity predicted for transitions to higher *fd* levels belonging to the same $5d$ state, however, is often too low.

The simulations can be improved by adjusting the *f-d* interaction parameters. When using the predicted $4f5d$ parameters according to Cowans's code, the calculated splitting turns out to be somewhat too large because the atomic parameters tend to overestimate this splitting. A better agreement can be obtained by using *fd* parameters smaller than the value calculated for the free ion. This is not unreasonable because in a solid the $5d$ electron is delocalized over the ligands (nephelauxetic effect) which will reduce the *f-d* coupling parameter in comparison to the free ion situation.[47] As an example, in Fig. 8(b) the calculated spectrum using *fd* parameters of 50% of the value predicted for the free ion is shown for $YPO_4:Pr^{3+}$, which gives the best agreement between the experimentally observed and calculated spectrum.

### C. $Nd^{3+}$

#### *1. Experiment*

$YPO_4$. Figure 12 shows the excitation spectrum of the $Nd^{3+}$ emission for $YPO_4$ doped with 1% $Nd^{3+}$ (solid line). Transitions to the $5d$ crystal-field components can be observed at 186 nm (A), 160 nm (B), and 156 nm (C). The transition to the fifth $5d$ level is expected at 140 nm, according to the crystal field splitting derived from the excitation spectrum of $YPO_4:Ce^{3+}$. However, at this energy the host lattice absorption is large and as a consequence the *fd* transition can not be observed.

The lowest *fd* excitation band consists of a zero-phonon line at 187.8 nm (denoted $A_1$) and a structured side band. Fine structure can be observed over an energy range of 9000 $cm^{-1}$ (189 to 162 nm). Other zero-phonon lines can be identified at 177.18 nm ($A_2$) and 169.67 nm ($A_3$), respectively, 3200 and 5700 $cm^{-1}$ from the *fd* onset ($A_1$). At wavelengths shorter than 162 nm, the fine structure disappears as the second $4f^2 5d$ excitation band is observed. Again, the absence of fine structure in the spectra of the higher energy *fd* bands is ascribed to line broadening due to fast photoionization.

The UV emission spectrum of $YPO_4:Nd^{3+}$ is shown in Fig. 13. Emissions are observed from the lowest *fd* level to the $4f^3$ states of $Nd^{3+}$. The transition to the ground state $^4I_{9/2}$ is observed at 189.5 nm, the Stokes shift is about 900 $cm^{-1}$. The absence of fine structure is due to the poor spectral resolution in emission.

$CaF_2$. The excitation spectrum of the $Nd^{3+}$ emission in $CaF_2$ doped with 0.001% $Nd^{3+}$ is shown in Fig. 14. The transition to the $^2E$ levels is observed at 179 nm ($A$), the transition to the $^2T_2$ ($B$) orbitals is observed at 133 nm. The $^4I_{9/2} \rightarrow {}^2E$ excitation band shows fine structure. The zero-phonon line $A_1$ is observed at 181.65 nm.

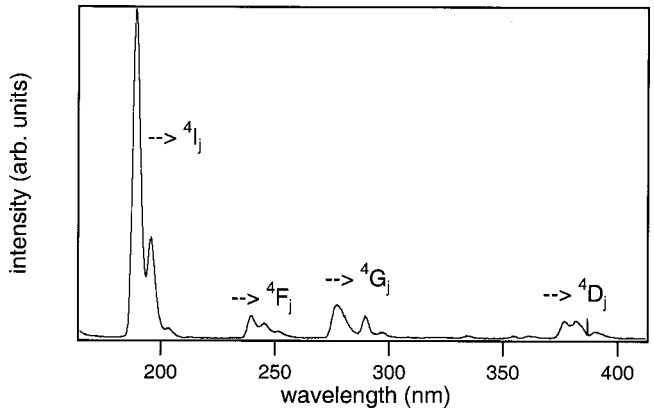


FIG. 13. UV emission spectrum of $YPO_4:Nd^{3+}$ 1% at 6 K, recorded for excitation at 160 nm.

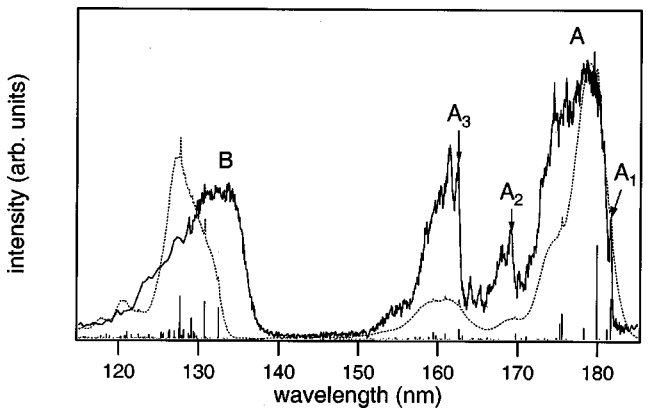


FIG. 14. Excitation spectrum of $CaF_2$:$Nd^{3+}$, $Na^+$ 0.001% at 6 K, recorded monitoring the $4f^25d^1 \rightarrow {}^4I_{9/2}$ emission at 190 nm.

The structure in the lowest *fd* excitation band resembles the structure for $Nd^{3+}$ in $YPO_4$. Structured bands are observed over an energy of 9000 $cm^{-1}$. The energy difference between line $A_1$ and $A_2$ is 4100 $cm^{-1}$, the energy difference between $A_1$ and $A_3$ is 6500 $cm^{-1}$. These splittings are approximately 15% larger than for $Nd^{3+}$ in $YPO_4$.

Figure 15 shows the emission spectrum of $CaF_2$:$Nd^{3+}$. Transitions are observed from the lowest *fd* level to the $4f^3$ states of $Nd^{3+}$. At 182 nm the transition to the ground state is observed, the Stokes shift is about 1200 $cm^{-1}$.

$LiYF_4$. Figure 16 shows the excitation spectrum of the $Nd^{3+}$ emission for $LiYF_4$ doped with 5% $Nd^{3+}$. The *fd* onset is at 178 nm ($A_1$), transitions to the second, third, fourth, and fifth $5d$ crystal-field components are observed at, respectively, 155 nm (B), 139 nm (C), 135 nm (D), and 129 nm (E), in agreement with the crystal-field splitting of the $5d$ orbitals as observed for $LiYF_4$:$Ce^{3+}$. The structure in the lowest *fd* excitation band is similar to the structure for $Nd^{3+}$ in $YPO_4$ and $CaF_2$.

The transition to the second $5d$ crystal-field component also shows splitting. The energy separation between band *F* (143 nm) and band *B* (155 nm) is 6000 $cm^{-1}$, similar to the energy separation between band $A_2$ and $A_1$ (6000 $cm^{-1}$). However, vibrational structure is not observed in these bands, as is generally the case for excitation bands corresponding to transitions to the higher crystal-field components.

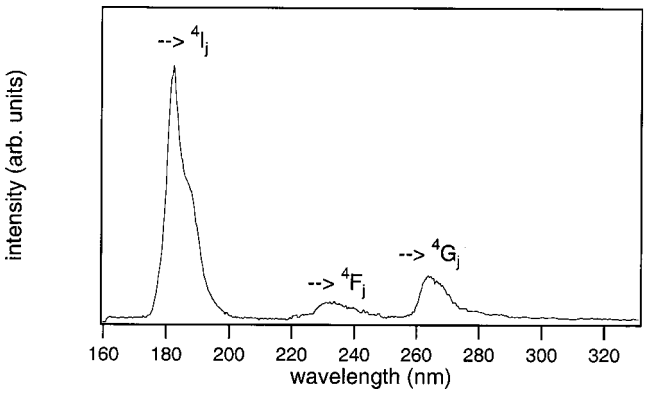


FIG. 15. UV emission spectrum of $CaF_2$:$Nd^{3+}$, $Na^+$ 0.001% at 6 K, recorded for excitation at 132 nm.

#### *2. Model*

The simulated spectra are shown as the dotted lines in Figs. 12, 14, and 16. Transitions to the $5d$ crystal-field components can be observed in both the simulated and experimental spectra. Fine structure is built on top of these in a complicated manner. Many of the electronic origins can be identified in the excitation spectra. These correspond quite closely to the calculations.

As was shown in the previous section for $Pr^{3+}$ in $YPO_4$, a better agreement between the experimentally observed energy levels and the calculations can be obtained by treating the *f-d* interaction parameters as adjustable parameters. Also the $5d$ crystal-field parameters decrease slightly due to the lanthanide contraction (by about 5% from $Ce^{3+}$ to $Tb^{3+}$). By reducing all *f-d* interaction parameters to 74% of the calculated values and reducing the $5d$ crystal field parameters to 98% of the $Ce^{3+}$ values, an excellent agreement between theory and experiment is obtained, as illustrated in Fig. 16(b) for $LiYF_4$:$Nd^{3+}$.

### D. $Sm^{3+}$

#### *1. Experiment*

$YPO_4$. Figure 17 shows the excitation spectrum of the $Sm^{3+}$ emission in $YPO_4$ doped with 1% $Sm^{3+}$. The first *fd* zero-phonon line is at 175.69 nm ($A_1$), the transitions to the second and third $5d$ crystal-field components are observed at 153 nm (*B*) and 147 nm (*C*). At 147 nm the host lattice starts to absorb and therefore transitions to the higher $4f5d$ levels cannot be observed.

Transitions corresponding to states involving the lowest $5d$ state show fine structure. Zero-phonon lines are observed at 175.69 nm ($A_1$), 171.53 nm ($A_2$), and 167.52 nm ($A_3$). The energy differences between $A_1$ and the zero-phonon lines $A_2$ and $A_3$ are 1350 and 2765 $cm^{-1}$, respectively. The fine structure pattern in the three bands is different. The first band shows a regular spacing between the lines of about 167 $cm^{-1}$. The second and third structured band have a zero-phonon line of highest intensity, phonon lines $A_2'$ and $A_3'$ are observed at about 340 $cm^{-1}$ higher in energy.

At lower energy a broad structureless excitation band is observed with a maximum at 179 nm. This transition is assigned to an oxygen-to-RE charge transfer transition, and is observed at lower energy than the *fd* transitions.

$CaF_2$. Figure 18 shows the excitation spectrum of the $Sm^{3+}$ emission in $CaF_2$ doped with 0.001% $Sm^{3+}$. The lowest *fd* excitation line is at 170.94 nm ($A_1$). Transition to states corresponding to the ${}^2T_2$ levels can be observed around 128 nm (*B*). At this energy also the $CaF_2$ host lattice starts to absorb (bandgap $E_g \sim 125$ nm), which can explain the lower intensity.

The lowest energy *fd* excitation band has fine structure and four zero-phonon lines can be identified. The lines $A_2$, $A_3$, and $A_4$ are separated from zero-phonon line $A_1$ by 1925, 3495, and 5095 $cm^{-1}$, respectively. The splitting is about

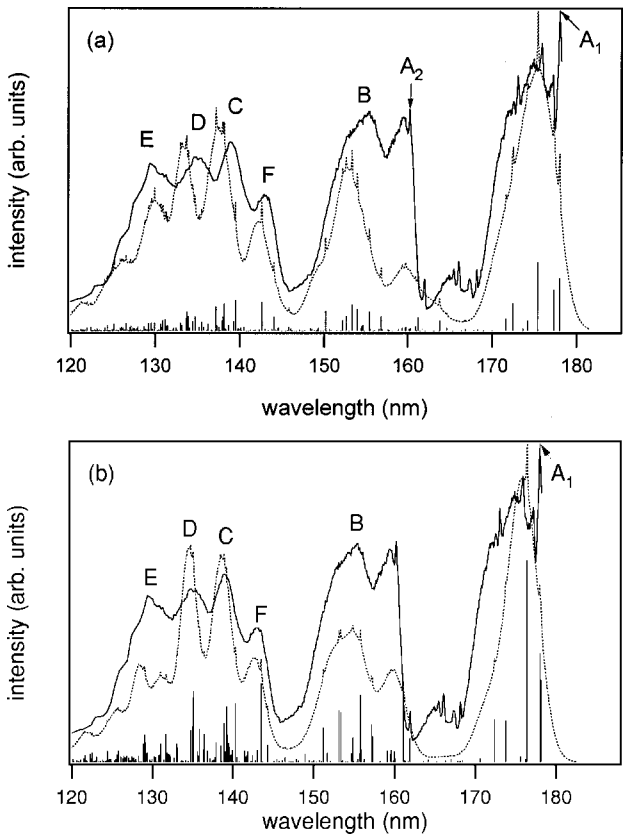


FIG. 16. Excitation spectrum of $LiYF_4$:$Nd^{3+}$ 5% at 6 K, recorded monitoring the $4f^2 5d^1 \rightarrow {}^4I_j$ emission at 182 nm. In (b) the calculated spectrum is presented (dotted line) for calculation with reduced *f-d* parameters (to 74% of the calculated value) and 5*d* crystal-field parameters (to 98% of the values fitted for $Ce^{3+}$).

20% larger than in $YPO_4$. In $CaF_2$ no $Sm^{3+}$CT band is observed. The fluoride→$Sm^{3+}$CT band is expected at higher energy in fluorides, due to the high electronegativity of the fluoride ion.

$LiYF_4$. The excitation spectrum of the $Sm^{3+}$ emission for $LiYF_4$ doped with 1% $Sm^{3+}$ is depicted in Fig. 19. The *fd* onset is observed at 167.78 nm ($A_1$), transitions to the higher crystal field components are observed at 149 nm (*B*), 132 nm (*C*), and 124 nm (*D*).

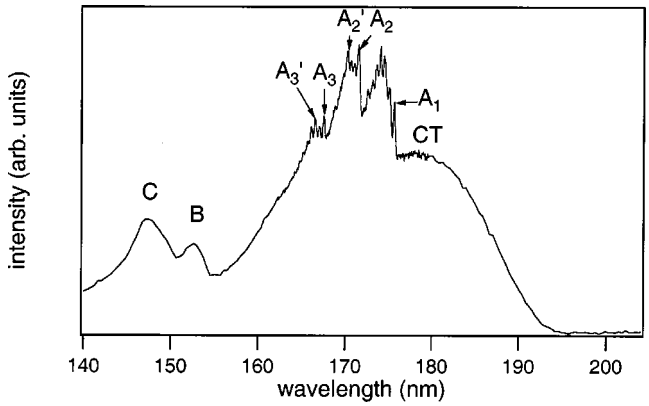


FIG. 17. Excitation spectrum of $YPO_4$ doped with 1% $Sm^{3+}$ at 6 K, recorded monitoring the ${}^4G_{5/2} \rightarrow {}^6H_{5/2}$ emission at 595 nm.

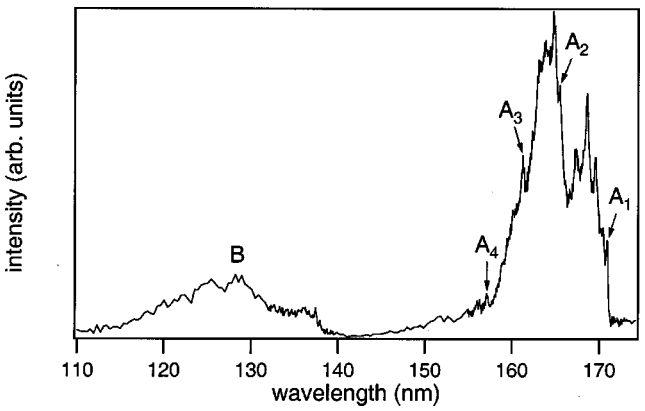


FIG. 18. Excitation spectrum of $CaF_2$:$Sm^{3+}$, $Na^+$ 0.001% at 6 K recorded monitoring all visible $4f$ emissions.

The lowest *fd* excitation band shows fine structure. The structure is similar to the structure observed for $Sm^{3+}$ in $YPO_4$ and $CaF_2$. Four bands are observed for the transition involving the lowest $5d$ state, zero-phonon lines are labeled $A_1$–$A_4$. $A_2$ is separated from $A_1$ by 1540 $cm^{-1}$, $A_3$ is separated from $A_1$ by 3065 $cm^{-1}$, and $A_4$ is separated from $A_1$ by 4815 $cm^{-1}$. The splitting is somewhat larger than the splitting observed in $YPO_4$ and somewhat smaller than the splitting observed in $CaF_2$.

The transitions to states involving the second $5d$ crystal-field component show a splitting similar to that of the first $5d$ crystal-field component. Three structureless bands can be observed with energy separations of, respectively, 1515 and 3140 $cm^{-1}$, in agreement with the separations found for the lowest-energy *fd* excitation bands.

### *2. Model*

To compare the experimentally observed structure with energy level calculations, only the case of $LiYF_4$:$Sm^{3+}$ was investigated (the parameters are known for $Sm^{3+}$ in $LiYF_4$, the structure is similar in the three host lattices and calculations for the $4f^4 5d$ configuration take more time than the ''simpler'' configurations discussed before). The values of the parameters are collected in Table II.

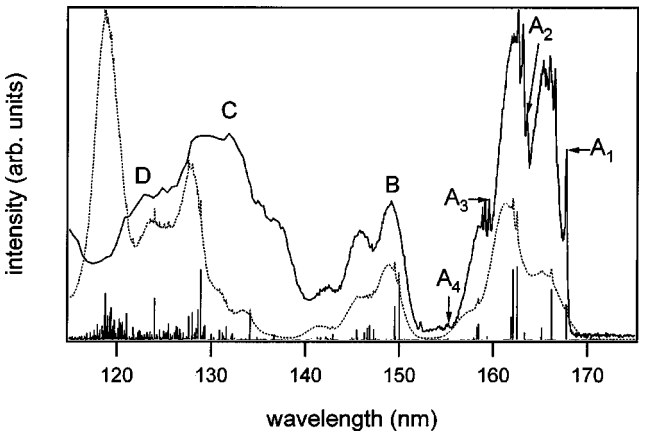


FIG. 19. Excitation spectrum of $LiYF_4$:$Sm^{3+}$ 1% at 6 K, recorded monitoring the emission at 605 nm.

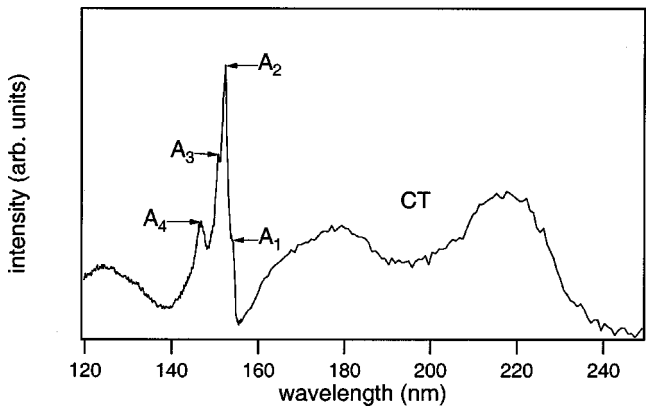


FIG. 20. Excitation spectrum of $YPO_4$ doped with 1% $Eu^{3+}$ at 6 K, recorded monitoring the $^5D_0 \rightarrow {}^7F_4$ emission at 700 nm.

The simulated spectrum is shown as the dotted line in Fig. 19. The agreement between the calculated spectrum and experimentally observed spectrum is quite good. The splitting and intensity pattern of the first *fd* excitation band is explained well by the model. Several zero-phonon lines can be identified in addition to those already identified before ($A_1$, $A_2$, $A_3$, and $A_4$). Also the splitting of the second *fd* excitation band is explained by the theory. The agreement at short wavelengths (<140 nm) is not as good as for the lowest-energy *fd* excitation bands. This might improve by reduction of the $5d$ crystal-field parameters, as was also observed for $LiYF_4$:$Nd^{3+}$ in Fig. 16(b).

### E. $Eu^{3+}$

$YPO_4$. For $Eu^{3+}(4f^6)$ the charge transfer state is at lower energy than the $4f^5 5d$ state, even in fluoride host lattices. Still, on the high-energy side of the broad CT excitation bands the fine structure in the $4f^5 5d$ excitation bands can be observed. In Fig. 20 the excitation spectrum of the $Eu^{3+}$ emission in $YPO_4$ doped with 1% $Eu^{3+}$ is shown. At 152 nm the transition to the lowest *fd* band is observed. At lower energy two broad bands are observed with maxima at 217 and 178 nm, due to oxygen-to-RE charge transfer transitions.

The transition to the lowest $5d$ crystal-field component is split into four bands. In contrast to the observation for the other ions, no zero-phonon lines and vibrational fine structure are observed for $Eu^{3+}$. This might be due to the position of the first *fd* band close to the host lattice absorption edge. The first maximum is observed at 154 nm ($A_1$), the second maximum is observed at 152 nm ($A_2$), at 715 $cm^{-1}$ higher energy. The energy difference between $A_1$ and $A_3$ at 151 nm is 1390 $cm^{-1}$, and between $A_1$ and $A_4$ (147 nm) 3170 $cm^{-1}$.

Transitions to the higher crystal-field components are expected at 134 nm and shorter wavelengths and are not observed in the spectrum, due to the strong host lattice absorption in this wavelength region.

$LiYF_4$. Figure 21 shows the excitation spectrum of $LiYF_4$ doped with 2% $Eu^{3+}$. A number of broad excitation bands are observed, some of them with fine structure. The positions of the bands agree with the low resolution spectrum reported in Ref. 48. The broad band observed at the low-energy side

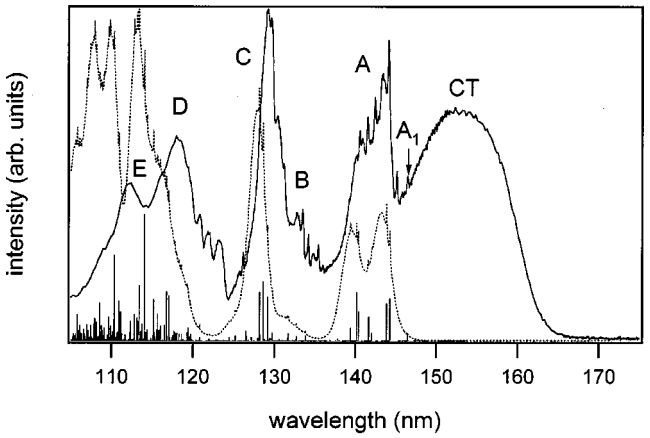


FIG. 21. Excitation spectrum of $LiYF_4$:$Eu^{3+}$ 1% at 6 K, recorded monitoring the $^5D_0 \rightarrow {}^7F_1$ emission at 590 nm.

of Fig. 21 has a maximum at 153 nm (CT) and is assigned to the fluoride-europium charge transfer band. At the high-energy side of this band, some structure is observed due to transitions to the lowest energy *fd* state of $Eu^{3+}$. To verify if these are the first *fd* zero-phonon lines the following expression can be used for calculating the position expected for the lowest *fd* level of a lanthanide ion in a particular compound:[49]

$$\Delta E(\mathrm{Ln},A) = \Delta E(\mathrm{Ce,free}) - D(A) + \Delta E^{\mathrm{Ln,Ce}} \qquad (1)$$

where $\Delta E(\mathrm{Ln},A)$ is the energy needed to excite an electron from the ground state multiplet in a certain lanthanide to its lowest $4f^{n-1}5d$ level, $\Delta E$ (Ce, free) is the *fd* excitation energy of the free $Ce^{3+}$ ion, $D(A)$ represents the depression value averaged over all lanthanides in a certain host lattice, and $\Delta E^{\mathrm{Ln,Ce}}$ is the energy difference of the lowest *fd* transition between a certain lanthanide ion and the cerium ion, averaged over all compounds *A*. According to this formula the *fd* onset of $Eu^{3+}$ in $LiYF_4$ can be expected around 145 nm, which is in close agreement with the onset of fine structure in Fig. 21 ($A_1$ at 146.4 nm). Transitions to the second, third and fifth crystal-field component can be observed at 129 (C), 118 (D), and 112 nm (E).

## V. GENERAL DISCUSSION

High-resolution $4f^n$-$4^{n-1}5d$ excitation spectra and a few (lower resolution) emission spectra have been recorded for the light lanthanide ions ($n<7$) incorporated in three different host lattices ($YPO_4$, $CaF_2$, and $LiYF_4$). In all three host lattices the relaxation in the $4f^{n-1}5d$ excited state is restricted resulting in small Stokes shifts and the observation of fine structure (zero-phonon lines and vibronic lines). The Stokes shift is smallest for the *fd* emission of lanthanide ions in $YPO_4$ (about 600 $cm^{-1}$) and somewhat larger in $CaF_2$ (about 900 $cm^{-1}$), and $LiYF_4$ (about 1300 $cm^{-1}$). In all three lattices fine structure is observed in the *fd* excitation spectra. The observation of fine structure is not often observed for $4f^n$-$4f^{n-1}5d$ transitions. Usually the *fd* spectra consist of broad structureless vibronic bands. For the comparison of

energy level calculations with experimentally observed energy levels the presence of fine structure is crucial. If all information on the position of individual energy levels is lost in a broad structureless band, no good comparison between theory and experiment is possible. This has determined the choice of the host lattices in which the excitation spectra of various lanthanide ions have been studied to the three host lattices in which fine structure is observed.

For the transitions to the lowest energy $5d$ crystal-field component fine structure is present (narrow zero-phonon line and vibronic lines). For transitions to energy levels corresponding to higher-energy $5d$ crystal-field components the fine structure has disappeared and broad structureless bands are observed. The absence of fine structure may be explained by fast photoionization. Because of this, most of the analysis is focussed on the structure found for transitions to the lowest energy $5d$ level. In all three host lattices the splitting between the lowest-energy $5d$ level and the next higher level is large (between 7000 and 20 000 $cm^{-1}$). This is a large enough window to observe many sharp lines corresponding to transitions to various $4f^{n-1}5d$ energy levels. For the higher-energy $5d$ levels still some broader spectral features can be observed and compared with the simulated spectrum.

Comparison of the fine structure observed for transitions to levels involving the lowest-energy $5d$ level show that the structure is very similar for one type of rare-earth ion in the three different host lattices. This is not unexpected, since the fine structure is due to interactions in the $4f^{n-1}$ core and the $f$-$d$ interactions and these are not strongly dependent on the host lattice. The splitting can clearly not be explained by assuming only a splitting of the $4f^{n-1}$ core superimposed on the splitting of the $5d$ state without $f$-$d$ coupling. The $f$-$d$ interaction in the $4f^{n-1}5d$ excited state has to be considered to explain the experimentally observed spectra. For the higher-energy $5d$ levels the structure (without sharp zero-phonon lines) often reflects the presence splitting patterns due to $4f^{n-1}$ and $f$-$d$ splitting which are similar to the patterns observed for the lowest $5d$ level. In other situations the presence of many overlapping bands arising from different $5d$ levels hampers the interpretation of the high-energy part of the spectrum.

To compare the experimentally observed spectra with energy-level calculations, a relatively simple model is used with as input parameters the splitting of the $5d$ states (by the crystal-field and spin-orbit coupling for the $5d$ electron), parameters for the splitting of the $4f^{n-1}$ core and parameters for Coulomb interaction between the $f$ and $d$ electrons. The parameters for the splitting of the $5d$ states are obtained from a best fit of the positions of $5d$ levels observed for $Ce^{3+}$ in the three host lattices. The Coulomb interaction and spin-orbit coupling parameters for the $4f^{n-1}$ core can (mostly) be found in the literature on the rare-earth ion with the $4f^{n-1}$ configuration and the parameters for the $f$-$d$ Coulomb interaction are calculated using Cowan's code (for the free ion). The agreement between the experimentally observed spectra and the energy-level calculations is good. The observed fine structure and relative intensities of the *fd* transitions are reproduced by the calculations. Still, further improvements can be made to the theory. As is discussed in Sec. IV B 2 the $f$-$d$ Coulomb interaction parameters are too large because they are calculated for the free ion. Due to delocalization of the $5d$ electron over the ligands for the lanthanide in a crystalline host, the $f$-$d$ interaction parameters can be expected to be reduced in a manner very similar to the reduction of the free ion Racah parameters ($A$, $B$, $C$) of the $3d$, $4d$, and $5d$ transition metal ions. When surrounded by ligands, the Racah parameters are reduced to typically 40 to 70 % of the free ion values due to the nephelauxetic effect. The reduction is stronger for more covalent ligands. To investigate this effect, energy level calculations were performed for $YPO_4$:$Pr^{3+}$ and $LiYF_4$:$Nd^{3+}$ with $F^k(fd)$ and $G^k(fd)$ as adjustable parameters. These Slater parameters are related to the Racah parameters and will also be reduced by the nephelauxetic effect. In order to prevent having five adjustable parameters all $F^k(fd)$ and $G^k(fd)$ parameters were reduced to the same amount. This approximation is not unreasonable, since all $f$-$d$ interaction parameters are expected to be reduced by the nephelauxetic effect. The best agreement is obtained for $f$-$d$ interaction parameters of 50% of the calculated values for $YPO_4$:$Pr^{3+}$ and 74% of the calculated values for $LiYF_4$:$Nd^{3+}$ [see Figs. 8(b) and 16(b)]. Indeed, a larger reduction is found for the more covalent ligands ($O^{2-}$ is more covalent than $F^-$).

A second reason for differences between the calculated and observed spectra is the rather unsatisfactory fit for the splitting of the $5d$ state as observed for $Ce^{3+}$. This is partly the reason for the mismatch of the energy level calculations and the experimental results at higher energies. Also, the crystal field splitting will become slightly smaller for the heavier lanthanide ions as a result of the lanthanide contraction. A good estimate of this effect can be obtained by comparing the excitation spectra of $Ce^{3+}$ and $Tb^{3+}$ in the different host lattices. Comparison indicates that the crystal field splitting for the $5d$ state of $Tb^{3+}$ (Ref. 44) is about 5% smaller than for $Ce^{3+}$. This effect has not been taken into account in the presently reported calculations, except for the calculations in Fig. 16(b) for $Nd^{3+}$ in $LiYF_4$. A slight (2%) reduction of the crystal field parameters resulted in a better agreement between the model and experiment, especially in the high energy region. In future research we will aim at improving the energy level calculations by allowing the $f$-$d$ Coulomb interaction to be smaller than the free ion value. A more realistic splitting of the $5d$ state can also be included. Finally, polarization dependent measurements will provide information on the symmetry of the levels and can provide support for the assignment of experimentally observed levels to calculated levels. Such a study has already been performed for $LiYF_4$:$Pr^{3+}$ and $YPO_4$:$Pr^{3+}$ (Refs. 41 and 43) but would also be very helpful for the other lanthanide ions.

## VI. CONCLUSION

In this paper, an overview of the $4f5d$ excitation and emission spectra of the light lanthanides ($Ce^{3+}$, $Pr^{3+}$, $Nd^{3+}$, $Sm^{3+}$, and $Eu^{3+}$) in $YPO_4$, $CaF_2$, and $LiYF_4$ has been given. In the excitation spectra the crystal-field splitting of the $5d$ electron can be clearly observed. Fine structure is observed for the transition to the lowest $5d$ crystal-field component.

For $Ce^{3+}$ it consists of a zero-phonon line and a vibronic side band. For the lanthanide ions with more than one $4f$ electron, the fine structure pattern is more complicated. It consists of several no-phonon lines with (superimposed) vibronic side bands. For the transitions to higher $5d$ crystal-field components no fine structure was observed. The electronic origins of these transitions are thought to be broadened due to photoionization to the conduction band and therefore unobservable.

The *fd* structure of the lanthanides is explained by extension of the standard calculations of $4f^n$ to include $4f^{n-1}5d$ states. Calculations of the positions of the $4f^{n-1}5d$ energy levels and intensities are compared with the experimental data. A good agreement is obtained between experimental and simulated spectra using parameters for the splitting of the $5d$ state (from the $Ce^{3+}$ spectra), the $4f^{n-1}$ splitting (from the literature), and the $f$-$d$ Coulomb interaction (calculated for the free ion using Cowan's code).

## ACKNOWLEDGMENTS

The authors wish to thank Dr. G. D. Jones of the University of Canterbury (Christchurch, New Zealand) for doing FTIR measurements on the $CaF_2$ crystals and many helpful discussions concerning the spectroscopy on doped $CaF_2$ crystals. The authors are grateful to Dr. P. Gürtler and Dr. S. Petersen from HASYLAB for the opportunity to use the excellent facilities for VUV spectroscopy at the DESY synchrotron, Hamburg (Germany) and their support whenever needed. The financial support of Philips Lighting, the New Zealand Marsden Fund (Contract No. UOC704), and INTAS (Contract No. 99-1350) is gratefully acknowledged.

*Electronic mail: L.vanpieterson@phys.uu.nl

[1] W. T. Carnall, G. L. Goodman, K. Rajnak, and R. S. Rana, J. Chem. Phys. **90**, 3443 (1989).
[2] C. Görller-Walrand and K. Binnemans, *Handbook on the Physics and Chemistry of Rare Earths*, edited by J. K. A. Gschneidner and L. Eyring (North-Holland, Amsterdam, 1996), Vol. 23, pp. 121–283.
[3] C. Görller-Walrand and K. Binnemans, *Handbook on the Physics and Chemistry of Rare Earths* (Ref. 2), Vol. 25, p. 101.
[4] G. H. Dieke, *Spectra and Energy Levels of Rare Earth Ions in Crystals* (Interscience, New York, 1968).
[5] R. T. Wegh, A. Meijerink, R. J. Lamminmäki, and J. Hölsä, J. Lumin. **87–89**, 1002 (2000).
[6] J. L. Ryan and C. K. Jøgensen, J. Phys. Chem. **70**, 2845 (1966).
[7] J. Rubio O., J. Phys. Chem. Solids **52**, 101 (1991).
[8] M. J. Freiser, S. Methfessel, and F. Holtzberg, J. Appl. Phys. **39**, 900 (1968).
[9] A. A. Kaplyanskii and P. P. Feofilov, Opt. Spectrosc. **13**, 129 (1962).
[10] A. A. Kaplyanskii, V. N. Medvedev, and P. P. Feofilov, Opt. Spectrosc. **14**, 351 (1963).
[11] A. Yanase and T. Kasuya, Prog. Theor. Phys. Suppl. **46**, 388 (1970).
[12] M. V. Eremin, Opt. Spectrosc. **26**, 317 (1969).
[13] L. L. Chase, Phys. Rev. B **2**, 2308 (1970).
[14] H. A. Weakliem, Phys. Rev. B **6**, 2743 (1972).
[15] T. Szczurek and M. Schlesinger, *Rare Earths Spectroscopy*, edited by B. Jezowska-Trzebiatowska, J. Legendziewicz, and W. Strek (World Scientific, Singapore, 1985).
[16] M. F. Reid, L. van Pieterson, R. T. Wegh, and A. Meijerink, Phys. Rev. B **62**, 14 744 (2000).
[17] W. Carnall, G. Goodman, K. Rajnak, and R. Rana, J. Chem. Phys. **90**, 3443 (1989).
[18] G. M. Williams, P. C. Becker, J. G. Conway, N. Edelstein, L. A. Boatner, and M. M. Abraham, Phys. Rev. B **40**, 4132 (1989).
[19] K. Lesniak, J. Phys.: Condens. Matter **2**, 5563 (1990).
[20] R. D. Cowan, *The Theory of Atomic Structure and Spectra* (University of California Press, Berkeley, 1981).
[21] B. G. Wybourne, *Spectroscopic Properties of Rare Earths* (Interscience, New York, 1965).
[22] A. Meijerink, R. T. Wegh, and L. van Pieterson, Proc.-Electrochem. Soc. **99–40**, 23 (2000).
[23] B. Henderson and G. F. Imbusch, *Optical Spectroscopy of Inorganic Solids* (Clarendon, Oxford, 1989).
[24] R. E. Thoma, C. F. Weaver, H. A. Friedman, H. Insley, L. A. Harris, and H. A. Yakel, Jr., J. Phys. Chem. **65**, 1096 (1961).
[25] D. W. Pack, W. J. Manthey, and D. S. McClure, Phys. Rev. B **40**, 9930 (1989).
[26] A. T. Aldred, Acta Crystallogr., Sect. B: Struct. Sci. **B40**, 569 (1984).
[27] U. Hahn, N. Schwentner, and G. Zimmerer, Nucl. Instrum. Methods **152**, 261 (1978).
[28] L. van Pieterson, M. Heeroma, E. de Heer, and A. Meijerink, J. Lumin. **91**, 177 (2000).
[29] G. M. Williams, N. Edelstein, L. A. Boatner, and M. M. Abraham, Phys. Rev. B **40**, 4143 (1989).
[30] J. Sytsma, D. Piehler, N. M. Edelstein, L. A. Boatner, and M. M. Abraham, Phys. Rev. B **47**, 14 786 (1993).
[31] R. J. Lang, Can. J. Res., Sect. A **14**, 127 (1936).
[32] B. Moine, B. Courtois, and C. Pedrini, J. Lumin. **45**, 248 (1990).
[33] C. Pedrini, F. Gaume-Mahn, and D. S. McClure, Rare Earths Mod. Sci. Technol. **3**, 165 (1982).
[34] R. L. Fuller and D. S. McClure, Phys. Rev. B **43**, 27 (1991).
[35] M. Raukas, S. A. Basun, W. van Schaik, W. M. Yen, and U. Happek, Appl. Phys. Lett. **69**, 3300 (1996).
[36] C. Pedrini, D. S. McClure, and C. H. Anderson, J. Chem. Phys. **70**, 4959 (1979).
[37] S. Lizzo, A. Meijerink, and G. Blasse, J. Lumin. **59**, 185 (1994).
[38] W. J. Manthey, Phys. Rev. B **8**, 4086 (1973).
[39] S. P. Jamison, R. J. Reeves, P. P. Pavlichuk, and G. D. Jones, J. Lumin. **83–84**, 429 (1999).
[40] C. M. Combes, P. Dorenbos, C. W. E. van Eijk, C. Pedrini, H. W. Den Hartog, and J. Y. Gesland, J. Lumin. **71**, 65 (1997).
[41] M. Laroche, S. Girard, J. Margerie, R. Monocorgé, M. Bettinelli, and E. Cavalli, J. Phys.: Condens. Matter **13**, 765 (2001).
[42] M. Marsman, J. Andriessen, and C. W. van Eijk, Phys. Rev. B **61**, 16 477 (2000).

[43] M. Laroche, J.-L. Doualan, S. Girard, J. Margerie, and R. Moncorgé, J. Opt. Soc. Am. B **17**, 1291 (2000).
[44] L. van Pieterson, M. F. Reid, G. W. Burdick, and A. Meijerink, Phys. Rev. B **65**, 045114 (2002) (the following paper).
[45] R. C. Naik, N. P. Kranjikar, and N. A. Narasimham, Solid State Commun. **38**, 389 (1981).
[46] K. D. Oskam, A. Houtepen, and A. Meijerink, J. Lumin. (to be published).
[47] H. A. Weakliem, Phys. Rev. B **6**, 1743 (1972).
[48] J. C. Krupa and M. Queffelec, J. Alloys Compd. **250**, 287 (1997).
[49] P. Dorenbos, J. Lumin. **91**, 91 (2000).